Inorganic Chemistry
Article
pubs.acs.org/IC

Anion Binding by Dimetallic Nickel(II) and Nickel(III) Complexes of a Face-to-face Bicyclam: Looking for a Bimacrocyclic Effect

Massimo Boiocchi,[†] Luigi Fabbrizzi,[*,‡] Nadia Fusco,[‡] Michele Invernici,[‡] Maurizio Licchelli,[‡] Antonio Poggi[‡]

[†] Centro Grandi Strumenti, Università di Pavia, via Bassi 21, 27100 Pavia, Italy

[‡] Dipartimento di Chimica, Università di Pavia, via Taramelli 12, 27100 Pavia, Italy

ABSTRACT: The dinickel(II) complex of the face-to-face bicyclam ligand α,α'-bis(5,7-dimethyl-l,4,8,l1-tetraazacyclotetradecan-6-yl)-o-xylene (L∩L) in a DMSO solution exists as a mixture of high- and low-spin forms and uptakes up to three halide and pseudohalide ions (X^-), according to three stepwise equilibria, whose constants were determined through spectrophotometric titration experiments. In the case of halides, the first anion goes into the intermetallic cavity, whereas pseudohalides first coordinate external metal centers. Comparison with equilibrium data for the complex with the macrocycle 5,7-dimethyl-1,4,8,11-tetraazacyclotetradecane (L), shows that the dinuclear complex $[Ni^{II}_2(L\cap L)]^{4+}$ displays affinity for the first halide distinctly higher than the mononuclear complex $[Ni^{II}(L)]^{2+}$, thus disclosing the existence of a *bimacrocyclic effect* for anion binding. Differential Pulse Voltammetry studies typically showed a three-peak profile: the most anodic pertaining to the $[Ni^{II}_2(L\cap L)]^{4+} \rightarrow Ni^{III}_2(L\cap L)]^{6+}$ two-electron process, then one originating from the $[Ni^{II}_2(L\cap L)X]^{3+} \rightarrow Ni^{III}_2(L\cap L)X]^{5+}$ two-electron process, and one deriving from the two two-electron half reactions $[Ni^{II}_2(L\cap L)X_2]^{2+} \rightarrow Ni^{III}_2(L\cap L)X_2]^{4+}$ and $[Ni^{II}_2(L\cap L)X_3]^{+} \rightarrow Ni^{III}_2(L\cap L)X_3]^{3+}$, taking place at nearly the same potential. The crystal and molecular structure of the $[Ni^{II}_2(L\cap L)(\mu\text{-}NCO)(NCO)_2]ClO_4$ complex salt showed a caterpillar arrangement of the three metal bound cyanate ions.

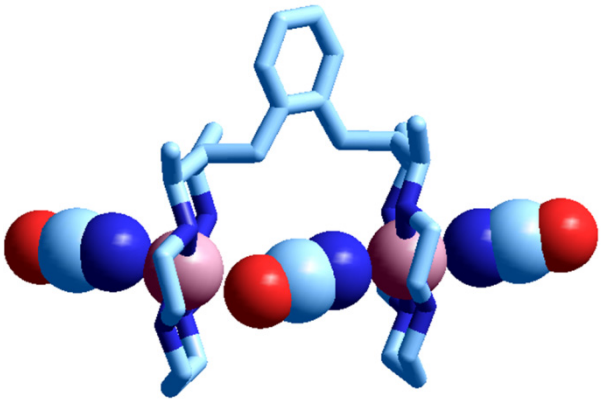

■ INTRODUCTION

Anion recognition results from the selective interaction with a given receptor, possibly of a concave shape, whose structural features fulfil the geometrical requirements of the anion.[1] Most anion receptors operate through electrostatic interactions, including hydrogen bonding. These interactions are not very energetic and the formation of stable complexes requires the design of highly preorganized receptors, whose positively charged binding points are strategically positioned inside the cavity.[2] On the other hand, coordinatively unsaturated metal complexes establish rather intense interactions with anions and can behave as efficient receptors for anions, operating in solvent of high polarity including water.[3] This is the case of complexes of labile metal ions (e.g. Cu^{II}) with

tetramines: branched (tren), linear (trien), cyclic (cyclam).[4] In general, the intensity of the metal-anion interaction varies according to the spectrochemical series, a circumstance which limits any design of selectivity.

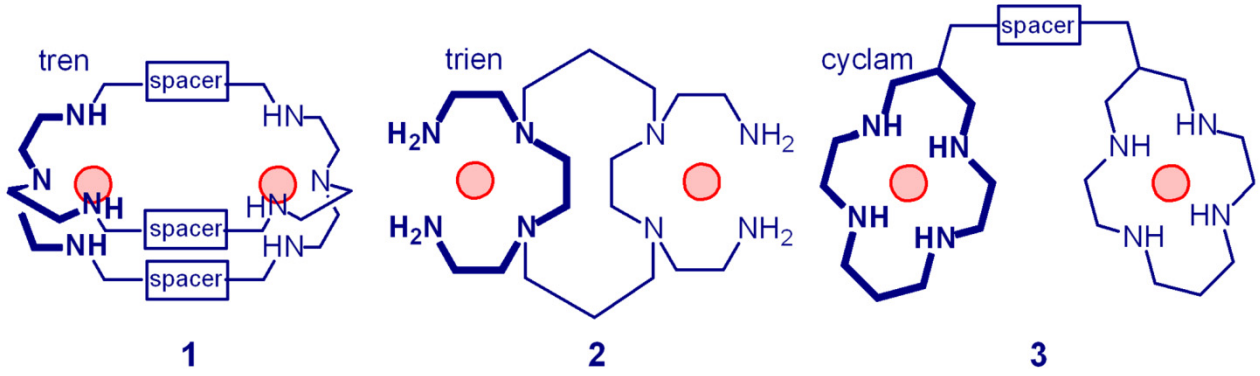

Scheme 1. Octamine ligands consisting of two distinct tetramine subunits, each capable to bind one metal center. Dimetallic complexes of the three tetramines can bind a single anion capable to bridge the two coordinatively unsaturated metal centers.

However, geometrical selectivity can be achieved through the design of *octamine* systems, consisting of two distinct *tetramine* subunits, each interacting with a metal center, which should remain coordinatively unsaturated. Three different types of octamine dinucleating ligands are shown in Scheme 1. Most investigated systems of this class are those of type **1** (*bistrens*), in which two tren subunits have been covalently linked by a variety of spacers.[5] The length of the spacer provides selectivity. For instance, when the spacer is 1,3-dimethylbenzene, the corresponding dicopper(II) bistren complex encapsulates polyatomic ambidentate anions capable of bridging the two metal centers, according to a selectivity based on the *bite length* (i.e. the distance of two consecutive donor atoms of the anion): the azide ion, among inorganic anions, forms the most stable inclusion complex.[6] The octamine **2**, bearing two trien subunits, shows a higher flexibility than **1** and its dicopper(II) complex is able to coordinate both mono- and poly-atomic anions bridging the two metals.[7] Notice that the tetramine subunits of octamines **1** and **2** forms with metal ions (e.g. Cu^{II}) *labile* complexes and are subject to demetallation in the presence of anion excess or under acidic conditions (due to the protonation of the amine groups). A further route to the design of dimetallic octamine receptors involves the covalent linking of two cyclam subunits (*bicyclams*, **3**).[8] In particular, the corresponding dimetallic complexes contain two *inert* metallocyclam moieties and will not undergo demetallation even under severe conditions. Moreover, if the two metallocyclam subunits are made to converge by an appropriate spacer, they can firmly include one anion, possibly establishing selective interaction.

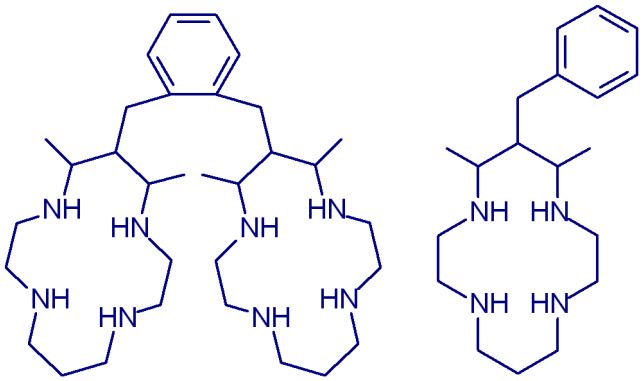

4 **5**

The bicyclam ligand **4** belongs to this family: it consists of two dimethylcyclam subunits bridged at the carbon center with an *ortho*-xylyl group, thus providing a face-to-face arrangement of the two macrocycles. A dinuclear complex of **4** is expected to include an ambidentate anion capable of encompassing the two metal centers, as sketched in formula **6**.

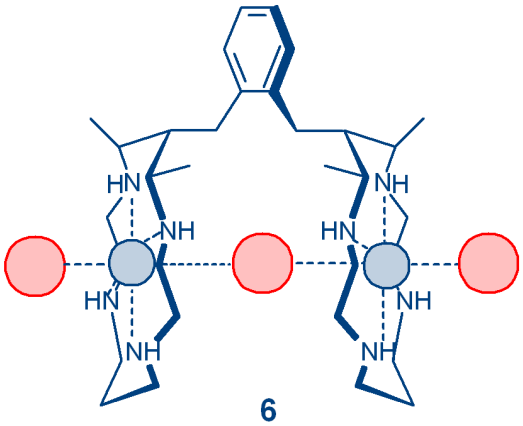

6

Ito *et al.* in 1993 reported the crystal structure, taken at room temperature, of the Ni^{II}_2(**4**)$Br_4 \cdot H_2O$ salt, in which the dimetallic complex $[Ni^{II}_2(\mathbf{4})(\mu\text{-}Br)Br_2]^+$ contained three bromide, one between the two metal centers, and two external.[9] The Br^- ion in the middle was located at two disordered positions and the distance between each Ni^{II} center and the closest Br^- position was 2.57 Å. On the other hand, the distance of each Ni^{II} center with the external bromide ion was rather large (2.88 Å), indicating a very weak interaction. The Authors suggested that 'each Ni^{II} ion is, therefore, in a square-planar four-coordinate geometry at 50% probability and in a five-coordinated square pyramidal environment at 50%.'[9] The puzzling point was that the Ni^{II}–N distance in both macrocyclic subunits was 2.01 ± 0.01 Å, a value intermediate between that expected for low-spin Ni^{II} (1.90−1.95 Å) and that expected for high-spin Ni^{II} (2.07−2.10 Å).

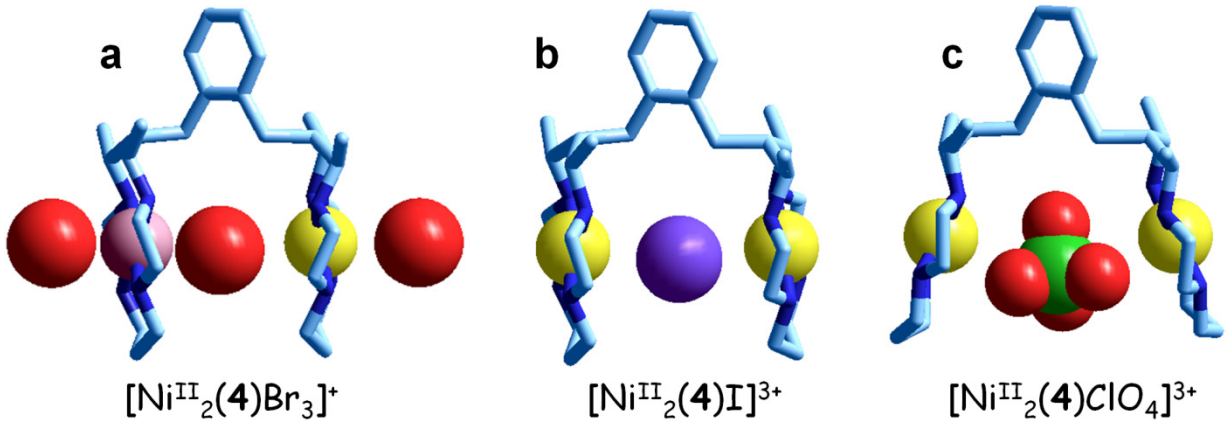

Figure 1. Crystal and molecular structures of (a) $[Ni^{II}_2(\mathbf{4})\ )(\mu\text{-Br})Br_2]^+$ (taken at 100 K); (b) $Ni^{II}_2(\mathbf{4})\ )(\mu\text{-I})]^{3+}$ (room temperature); (c) $[Ni^{II}_2(\mathbf{4})](\mu\text{-}ClO_4)]^{3+}$ (room temperature), all from ref 10. Color of the spheres in the metallocyclam subunits indicates the spin state of Ni^{II}: yellow, low-spin; blue-violet, high-spin.

In 2005, Endicott *et al.* made clear the point determining the X-ray structure of $[Ni^{II}_2(\mathbf{4})\ )(\mu\text{-Br})Br_2]ClO_4$ salt at 100 K.[10] The structure, displayed in Figure 1a, showed the presence of one high-spin Ni^{II} (blue-violet sphere) with long Ni^{II}–N bonds (2.07 Å) and of one low-spin Ni^{II} (yellow sphere) with short Ni^{II}–N bonds (1.96 Å). Moreover, the high-spin Ni^{II} established two short bonds with Br^- (2.62 Å inside the dimer, 2.71 Å outside), whereas long Ni^{II}–Br distances were observed for the low-spin metal center (3.32 Å inside, 3.07 Å outside). The $Ni^{II}\cdots Ni^{II}$ distance was 5.80 Å.

Furthermore, the Authors demonstrated that nickel(II) complexes of **4** showed an extreme versatility in the electronic behavior, depending upon the nature of the anion enclosed between the two facing metallocyclam subunits. Figure 2b shows the room temperature structure of the complex salt $[Ni^{II}_2(\mathbf{4})\ )(\mu\text{-I})](ClO_4)_3$. Both Ni^{II} ions (yellow spheres) are low-spin and the iodide ion in the middle is weakly coordinated. The $Ni^{II}\cdots Ni^{II}$ distance is 6.38 Å. The complex in Figure 1c, $[Ni^{II}_2(\mathbf{4})](\mu\text{-}ClO_4)]^{3+}$ (from the salt $[Ni^{II}_2(\mathbf{4})](\mu\text{-}ClO_4)](ClO_4)_3\cdot C_2H_5OH\cdot H_2O$) exhibits a quite similar structure, with a perchlorate ion included between two low-spin Ni^{II} ions (yellow spheres, $Ni^{II}\cdots Ni^{II}$ distance 7.20 Å).

We considered that the behavior of the $[Ni^{II}_2(\mathbf{4})]^{4+}$ complex as an anion receptor in solution could deserve an investigation. Present study has been addressed to the interaction of $[Ni^{II}_2(\mathbf{4})]^{4+}$ with halides and pseudohalides (NCO^-, NCS^-, N_3^-) in a DMSO solution and the corresponding stepwise binding constants have been determined through spectrophotometric titration experiments. Moreover, the crystal and molecular structure of the dinuclear complex $[Ni^{II}_2(\mathbf{4})\ (\mu\text{-NCO})(NCO)_2]^+$, containing two high-spin Ni^{II} centers, has been determined. Moreover, the Ni^{II}-to-Ni^{III} oxidation process in DMSO has been investigated through voltammetric techniques, in the absence and in the presence of added aliquots of poorly reducing anions: Cl^-, NCO^-, $N_3^-$and NO_3^-, to evaluate the capability of the $[Ni^{II}_2(\mathbf{4})]^{4+}$ receptor to act as an electrochemical anion sensor. Finally, in order to

verify the existence of cooperative effects in the solution behavior of $[Ni^{II}_2(\mathbf{4})]^{4+}$, if any, comparative spectrophotometric and voltammetric studies have been carried out on the mono-nuclear complex $[Ni^{II}(\mathbf{5})]^{2+}$, under the same conditions.

■ RESULTS AND DISCUSSION

Nature of the mononuclear $[Ni^{II}(5)]^{2+}$ and dinuclear $[Ni^{II}_2(4)]^{4+}$ complexes in DMSO solution. Nickel(II) complexes with cyclam and cyclam-like macrocycles exist in solution as an equilibrium mixture of two species: a high-spin complex of octahedrically elongated geometry and a low-spin complex of square planar geometry,[11] as illustrated in Figure 2.

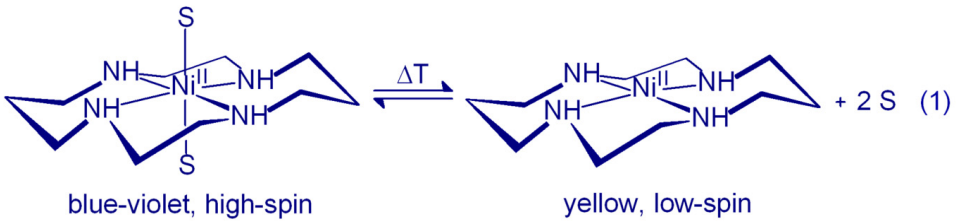

Figure 2. The blue-to-yellow conversion in nickel(II) complexes of cyclam and cyclam-like macrocycles. The position of the equilibrium depends upon the coordinating tendencies of the solvent S: the more coordinating S, the higher the concentration of the high-spin complex.

Two solvent molecules participate in the equilibrium, as they occupy the axial positions of the elongated octahedral high-spin complex. It derives that coordinating solvents favor the formation of the octahedral species and displaces the equilibrium (1) to the left-side. For instance, in the case of cyclam, the high-spin complex is present at 29% in water and at 78% in the more coordinating solvent MeCN.[12]

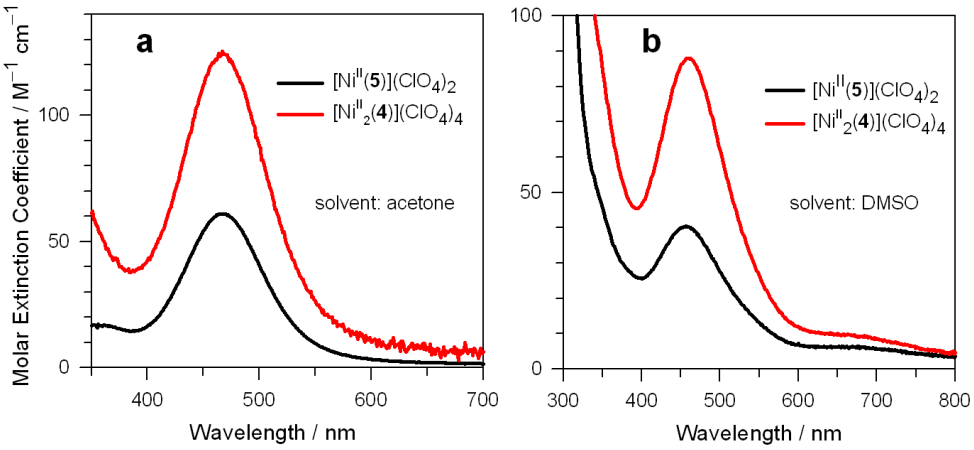

Figure 3. (a) spectra in acetone solution of $[Ni^{II}_2(\mathbf{4})](ClO_4)_4$ (red line) and of $[Ni^{II}(\mathbf{5})](ClO_4)$ (black line); (b) spectra in DMSO solution of $[Ni^{II}(\mathbf{4})](ClO_4)_2$ (red line) and of $[Ni^{II}(\mathbf{5})](ClO_4)_2$ (black line).

Acetone is a typically non-coordinating solvent and promotes the formation of 100% of the square planar complex. Figure 3a compares the spectra in acetone of the $[Ni^{II}_2(\mathbf{4})]^{4+}$ dinuclear

complex and of the corresponding mononuclear species $[Ni^{II}(\mathbf{5})]^{2+}$. Both complexes present a band centered at 468 nm, corresponding to a low-spin square planar chromophore. Noticeably, the molar extinction coefficient ε for the dinuclear complex (124 M^{-1} cm^{-1}) is twice of that of that observed for the mononuclear complex $[Ni^{II}(\mathbf{5})]^{2+}$ (62 M^{-1} cm^{-1}). On the other hand the solvent used in this study, DMSO, is a coordinating medium and is expected to favor the formation of the octahedral high-spin complex. Both mononuclear and dinuclear complexes in DMSO show bands centered at 460 nm (ε = 40 and 93 M^{-1} cm^{-1}, respectively), which are distinctly less intense than in acetone, thus suggesting the occurrence of a blue-to-yellow equilibrium. Notice that the intense absorption band centered at 460 nm obscures the bands of the high-spin octahedral form of both mono- and di-nuclear complexes. Thus, only a weak band at ~ 700 nm can be observed.

On tentatively assuming that the ε value of the band of the yellow complex is the same in acetone and in DMSO (a quite reasonable assumption for *d-d* transitions), $\varepsilon_{DMSO}/\varepsilon_{acetone} \times 100$ = 65% should give an approximate value of the concentration of the square planar form of the mono-nuclear complex $[Ni^{II}(\mathbf{5})]^{2+}$. Also the spectrum of the dinuclear complex in DMSO (red line in Figure 2b) indicates a dominating presence of the low-spin yellow chromophore. From the expression $\varepsilon_{DMSO}/\varepsilon_{acetone} \times 100$, a concentration of the yellow square chromophore of 75% can be calculated. It is suggested that the spin conversion equilibrium involves a dinuclear complex containing a high-spin metallocyclam and a low-spin metallocyclam on the left side (**a**) and a dinuclear complex with two low-spin metallocyclam on the right side (**b**), as tentatively sketched in Figure 4.

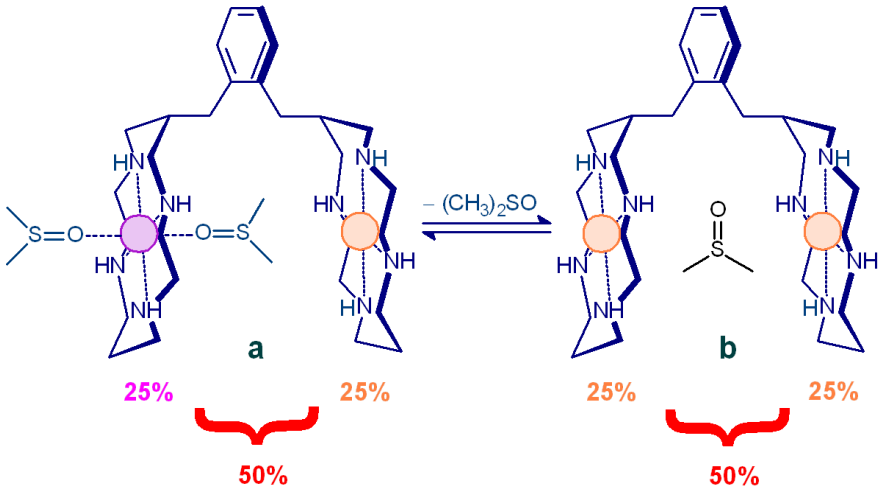

Figure 4. The hypothesized spin conversion equilibrium involving complex **a** (one high-spin octahedral subunit and one low-spin square-planar subunit) and complex **b** (two low-spin square-planar subunits).

The value of $\varepsilon_{DMSO}/\varepsilon_{acetone} \times 100$ = 75% should therefore result from the presence in solution of 50% of the complex **a** (mixed spin state) and 50% of the complex **b** (all low-spin state). The presence of an all high-spin complex cannot be excluded in principle, but in such a complex *two* coordinated

DMSO molecules should be probably present in the space between the two metallocyclam subunits, a circumstance highly disfavored by sterical repulsions.

Crystal and molecular structure of the $[Ni^{II}_2(4)(\mu\text{-}NCO)(NCO)_2]ClO_4\cdot 2.5(H_2O)$ complex salt. Figure 5 shows the molecular structure of the $[Ni^{II}_2(4)(\mu\text{-}NCO)(NCO)_2]ClO_4\cdot 2.5H_2O$ complex salt.

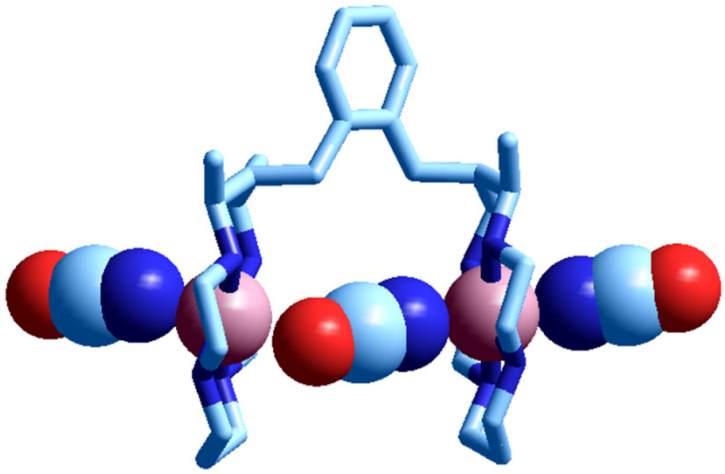

Figure 5. The crystal and molecular structure of the $[Ni^{II}_2(\mathbf{4})(\mu\text{-}NCO)(NCO)_2]ClO_4\cdot 2.5H_2O$ complex salt. The perchlorate anion as well water molecules and hydrogen atoms have been omitted for clarity.

Each nickel(II) ion is coplanarly chelated by the cyclam macrocycle, arranged in a *trans*-III configuration,[13] the most common conformational arrangement found in Ni^{II}-cyclam complexes.[14] The Ni^{II}–N_{amine} distances observed for both metallocyclam subunits (2.07−2.08 Å) are those expected for a high-spin center.[15]

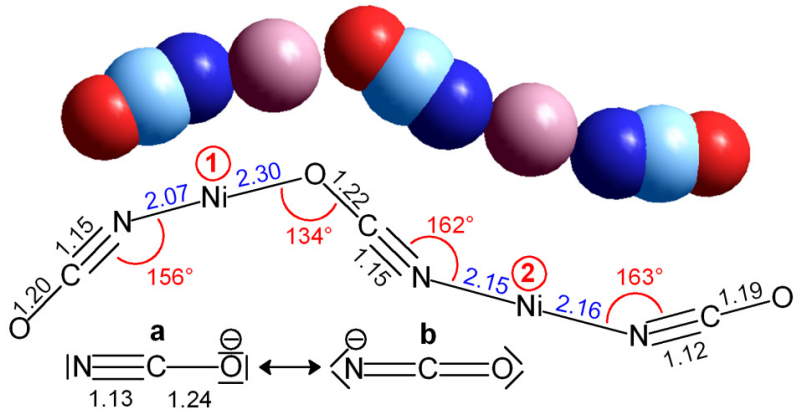

Figure 6. Bond distances (Å) and bond angles in the chain of Ni^{II} and cyanate ions in the $[Ni^{II}_2(\mathbf{4})(\mu\text{-}NCO)(NCO)_2]^+$ complex, whose complete structure is shown in Figure 4. The N−C and C−O distances in the ionic NCO^- is shown in the bottom of the Figure.

Geometrical aspects of the coordination of cyanate to the Ni^{II} ions are illustrated in Figure 6. Both Ni^{II} ions experience a distorted octahedral geometry with, however, quite different features. The metal center labeled with ② in the structural formula in Figure 6 is axially coordinated to the nitrogen atoms of the two cyanate ions with similar Ni^{II}–N distances of 2.15 and 2.16 Å, to give rise to an axially elongated octahedron. On the other hand, the Ni^{II} ion labeled with ① is bound to the nitrogen atom of an NCO^- ion with a relatively short distance (2.07 Å, the same as the Ni^{II}–N_{amine}

bond), but is loosely bound to the oxygen atom of NCO^- (Ni^{II}①−O distance 2.30 Å), originating an uniaxially elongated octahedron. Ni^{II} and NCO^- ions are arranged according to a caterpillar-like shape, which results from the different hybridization of the nitrogen and oxygen atoms of the cyanate ion. Bonding in NCO^- can be described by resonance diagram shown in the bottom of Figure 6. Canonical form **a** is the major contributor because the negative charge is located on the more electronegative atom, which agrees with the experimentally determined bond distances (d(N≡C) appreciably shorter than d(C−O), see Figure 6). Thus, the nitrogen atom should have a prevailing *sp* character and the oxygen atom a dominant sp^3 nature. This may account for the fact that the C−O−Ni^{II}① angle (134°) is distinctly smaller than the C−N−Ni^{II}① angle (156°) and C−N−Ni^{II}② angles (162° and 163°). The Ni^{II}①···Ni^{II}② distance is 6.43 Å, intermediate between those observed for the $[Ni^{II}_2(\mathbf{4}))$ $)(\mu\text{-Br})Br_2]^+$ complex (5.80 Å) and the $[Ni^{II}_2(\mathbf{4})(\mu\text{-}ClO_4)]^{3+}$ complex (7.20 Å). Thus, it appears that there is no steric impediment to a closer approach of the two cyclam subunits, which could favor the formation of a strong Ni^{II}−O bond. This suggests that the long Ni^{II}①−O distance has to be ascribed to an intrinsically low affinity of the metal center for the NCO^- oxygen atom.

Many examples have been reported of sequences of three or more thiocyanate anions interfaced by two transition metal cations (including Co^{II}, Ni^{II} and Cu^{II}). The described complex is the first example of three NCO^- anions interfaced by two Ni metal cations with the sequence: O–C≡N–Ni–O–C≡N–Ni–N≡C–O. A similar caterpillar-like arrangement occurs only for the bis(3-aminopyridine)-di-cyanate-copper(II) complex,[16] where square-planar Cu^{II} centers establish two additional and very weak axial interactions with the oxygens of adjacent CNO^- ions (Cu–O = 2.66 Å) originating infinite chains of the type: –Cu–O–C≡N–Cu–N≡C–O–Cu–O–C≡N–Cu–. These chains exhibit C–N–Cu^{II} and C–O–Cu^{II} angles of 161° and 119°, respectively, to be compared with the values observed in the Ni^{II} complex reported here: 163°, 162°, and 156° for C–N–Ni^{II} and 134° for C–O–Ni^{II}.

Anion uptake by the mononuclear $[Ni^{II}(5)]^{2+}$ and dinuclear $[Ni^{II}_2(4)]^{4+}$ complexes in DMSO solution. The affinity toward anions of the envisaged nickel(II) complexes was investigated through spectrophotometric titration experiments in DMSO solution. In a typical experiment, a solution of the metal complex perchlorate salt (either mono- or di-nuclear) was titrated with a solution of the tetrabutylammonium salt of the chosen anion (halide, pseudohalide). Spectrophotometric data were processed by a non-linear least-squares program,[17] in order to single out species present at the equilibrium and to determine their association constants. Figure 7a shows

the spectra taken over the course of the titration of a solution 5×10^{-3} M in the mononuclear complex salt $[Ni^{II}(\mathbf{5})](ClO_4)_2$ with a solution of $[Bu_4N]I$.

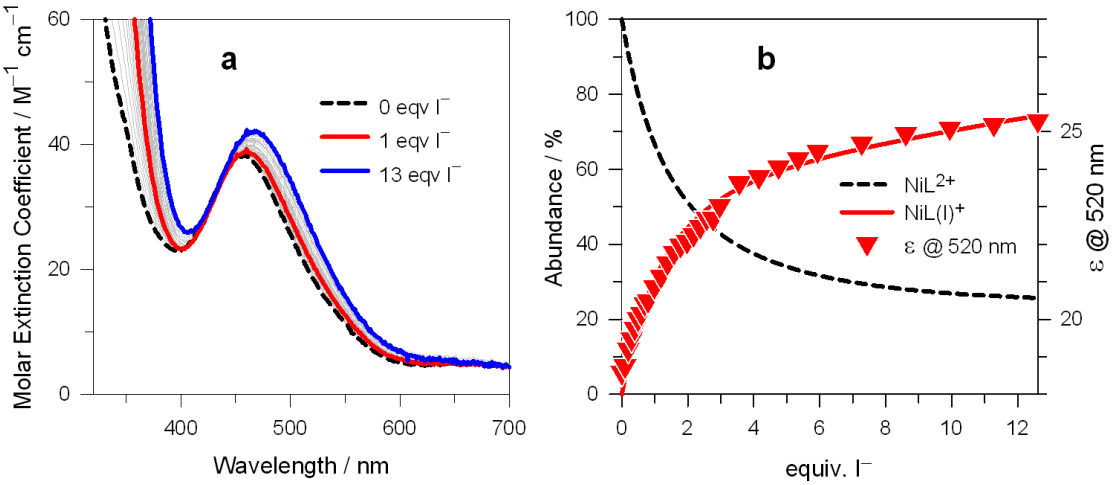

Figure 7. (a) Spectra taken over the course of the titration of a DMSO solution 5×10^{-3} M in $[Ni^{II}(\mathbf{5})](ClO_4)_2$ with $[Bu_4N]I$, at 25 °C; (b) symbols: Molar Extinction Coefficients (ε) taken at a selected wavelength; lines: concentration profiles of the complex species at the equilibrium over the course of the titration (L = **5**)..

On iodide addition, the band centered at 455 nm, pertinent to the square-planar low-spin complex, present at the equilibrium at 65%, undergoes a slight increase in intensity and a moderate red-shift. Best fitting of titration data was obtained by assuming the occurrence of a single equilibrium, eq. (2), to which a binding constant log $K = 1.87 \pm 0.02$ corresponded.

$$[Ni^{II}L]^{2+} + I^- \leftrightarrows [Ni^{II}L(I)]^+ \qquad (2)$$

It is suggested that the $[Ni^{II}L(I)]^+$ species exhibits a square-pyramidal geometry: the apically bound iodide does not exert a coordinative interaction strong enough to induce a complete spin-crossover and the mixture of five-coordinated low-spin and high-spin forms is maintained. This explains the minor modification of spectral features. The geometrical aspects of eq.(1) are pictorially illustrated in Figure 8b.

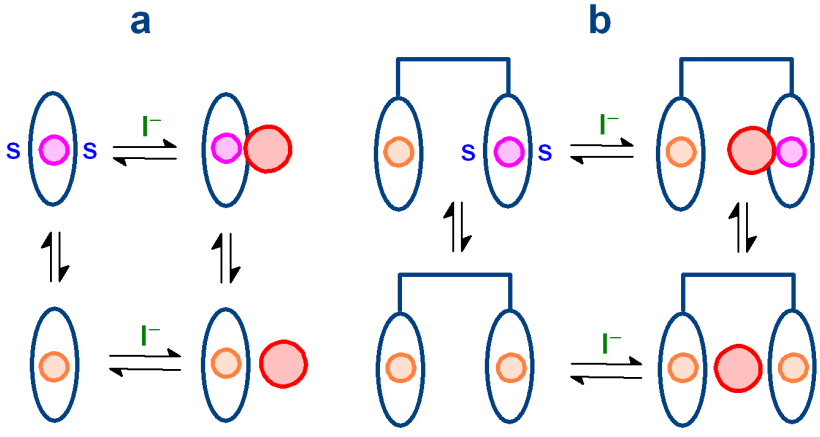

Figure 8. Pictorial description of the interaction of iodide with: (a) $[Ni^{II}(\mathbf{5})]^{2+}$ and (b) $[Ni^{II}_2(\mathbf{4})]^{4+}$.

Notice that the $[Ni^{II}L(I)]^+$ complex is poorly stable and, even on addition of a large excess of I^- (~ 13 equiv.) it forms only at ~ 75% (see Figure 8a).

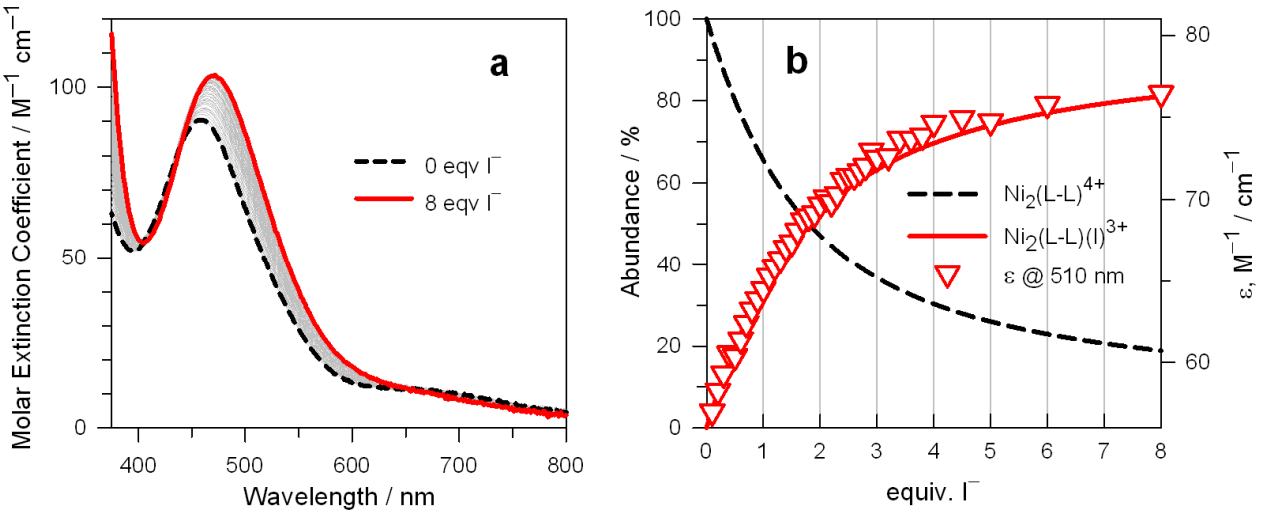

Figure 9. (a) Family of spectra taken over the course of the titration of a DMSO solution 5.10×10^{-4} M in $[Ni^{II}_2(\mathbf{4})](ClO_4)_4$ with $[Bu_4N]I$, at 25 °C; (b) symbols: Molar Extinction Coefficients (ε) taken at selected wavelengths; lines: concentration profiles of the complex species at the equilibrium over the course of the titration (L∩L = **4**).

Figure 9 shows the spectra taken over the course of the titration of a solution 5×10^{-3} M in the dinuclear complex salt $[Ni^{II}_2(\mathbf{4})](ClO_4)_4$ with $[Bu_4N]I$, at 25 °C. The spectral pattern is similar to that observed for the mononuclear analogue, involving a moderate increase and red-shift of the absorption band of the yellow chromophore. Best fitting of titration data was obtained by assuming the occurrence of eq.(3), to which a log $K = 2.22 \pm 0.02$ corresponded (L∩L = **4**).

$$[Ni^{II}_2L\cap L]^{2+} + I^- \leftrightarrows [Ni^{II}_2L\cap L(I)]^+ \qquad (3)$$

The hypothesized structural features of eq.(3) are illustrated in Figure 8b. It is suggested that the I^- ion is included between the two metallocyclam subunits, according to the arrangement observed in the solid state (Figure 1b). Also in the present case, iodide binding does not substantially modify the the concentration of the high-spin and low-spin forms. In any case, the weak coordinative interaction of I^- with the two Ni^{II} ions may account for the slightly higher value of log K of $[Ni^{II}_2(\mathbf{4})]^{4+}$ with respect to $[Ni^{II}(\mathbf{5})]^{2+}$, which establishes only one interaction (0.3 log units). The behavior of iodide is unique among investigated halides. Figure 10 shows the spectra taken during the titration with chloride of a solution of the mononuclear complex $[Ni^{II}(\mathbf{5})]^{2+}$.

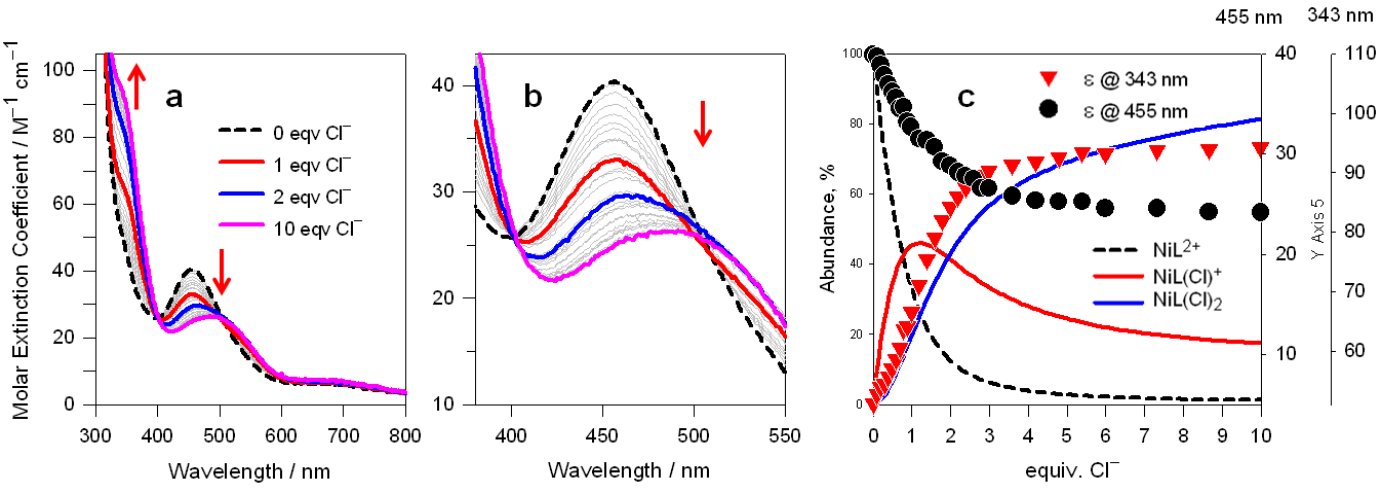

Figure 10. (a) Spectra taken over the course of the titration of a DMSO solution 5.0 × 10^{-4} M in $[Ni^{II}(\mathbf{5})](ClO_4)_2$ with $[Bu_4N]Cl$, at 25 °C; (b) spectra taken in the visible region (c) symbols: Molar Extinction Coefficients (ε) taken at selected wavelengths; lines: concentration profiles of the complex species at the equilibrium over the course of the titration.

It is observed (Figure 10a) that, on chloride addition, the band at 455 nm, pertinent to the low-spin species, decreases substantially and undergoes red-shift, whereas bands at 700 nm and, in particular, at 330 nm, pertinent to the high-spin complex, develop. However, even on addition of 10-fold excess of anion, the band of the yellow chromophore does not disappear, but reaches a steady value (see filled circles in Figure 10c). This indicates that diamagnetic species are present at the equilibrium in substantial concentration over the entire titration. Best fitting of titration data was obtained by assuming the occurrence of the two following stepwise equilibria:

$$[Ni^{II}L]^{2+} + Cl^- \leftrightarrows [Ni^{II}L(Cl)]^+ \qquad (4)$$

$$[Ni^{II}L(Cl)]^+ + Cl^- \leftrightarrows [Ni^{II}L(Cl)_2] \qquad (5)$$

to which the following stepwise constants corresponds: log K_1 = 2.7 ± 0.1 and log K_2 = 2.2 ± 0.3. Structural changes associated to eq.(4) and eq(5) are tentatively illustrated in Figure 11.

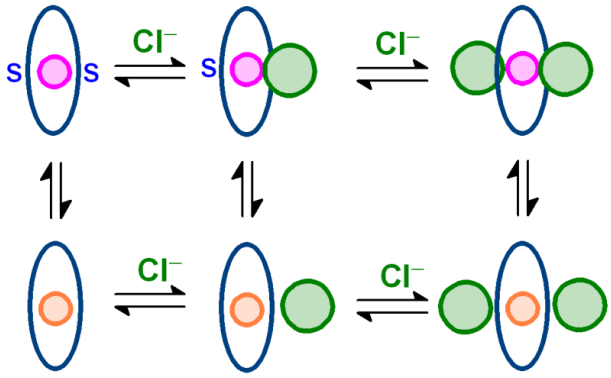

Figure 11. Hypothesized changes in the coordination sphere of the $[Ni^{II}(\mathbf{5})]^{2+}$ complex on titration with Cl^-.

In particular, it is assumed that the high/low-spin equilibrium is maintained during the stepwise addition of chloride ions, but the concentration of the high-spin form progressively prevails. For $[Ni^{II}L(Cl)_2]$ two octahedrically elongated complexes co-exist, whose spin state, whether high or low, is determined by the $Ni^{II}\cdots Cl$ distance, shorter for high-spin, longer for low-spin. Such a situation has been postulated to occur for complexes of the type $[Ni^{II}(macrocycle)(H_2O)_2]^{2+}$ in aqueous solution,[18] but it has been not observed yet in the presence of coordinating anions in non-aqueous solutions.

Figure 12 shows the spectra taken over the course of the titration of a solution 5×10^{-3} M in the dinuclear complex salt $[Ni^{II}_2(\mathbf{4})](ClO_4)_4$ with $[Bu_4N]C$, at 25 °C. The spectral pattern is analogous to that observed for the mononuclear counterpart, involving decrease, but not disappearance of the yellow chromophore. Moreover, a band at 350 nm, characteristic of the blue-violet chromophore distinctly develops on chloride addition.

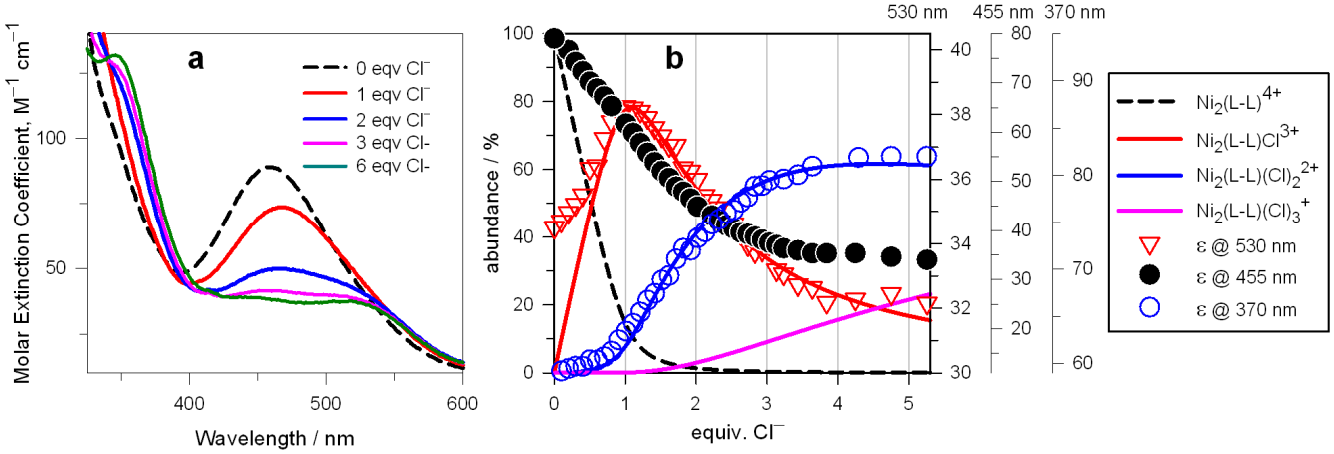

Figure 12. (a) Spectra taken over the course of the titration of a DMSO solution VALUE $\times 10^{-4}$ M in $[Ni^{II}_2(\mathbf{4})](ClO_4)_4$ with $[Bu_4N]Cl$, at 25 °C; (b) symbols: Molar Extinction Coefficients (ε) taken at selected wavelengths; lines: concentration profiles of the complex species at the equilibrium over the course of the titration.

Best fitting of titration data was obtained by assuming the occurrence of three stepwise equilibria, to which the following constants corresponded: $\log K_1 = 4.20 \pm 0.01$, $\log K_2 = 2.48 \pm 0.02$, $\log K_3 = 1.46 \pm 0.04$.

$$[Ni^{II}_2(L\cap L)]^{4+} + Cl^- \leftrightarrows [Ni^{II}_2(L\cap L)Cl]^{3+} \qquad (6)$$

$$[Ni^{II}_2(L\cap L)Cl]^{3+} + Cl^- \leftrightarrows [Ni^{II}_2(L\cap L)Cl_2]^{2+} \qquad (7)$$

$$[Ni^{II}_2(L\cap L)Cl_2]^{3+} + Cl^- \leftrightarrows [Ni^{II}_2(L\cap L)Cl_3]^{+} \qquad (8)$$

There is no way, from spectrophotometric data, to assess where the first Cl- ion goes (eq. (6)), whether in the intermetallic cavity or in one of the two external positions. The crystal structure of

the dinuclear complex salt $[Ni^{II}_2(\mathbf{5})(\mu\text{-}Cl)(ClO_4)](ClO_4)_2{\cdot}H_2O$, shown in Figure 13, suggests that the first Cl^- prefers to occupy the inter-metallocyclam space. In solution, the external perchlorate ion of the crystalline complex, would be probably replaced by a DMSO molecule.

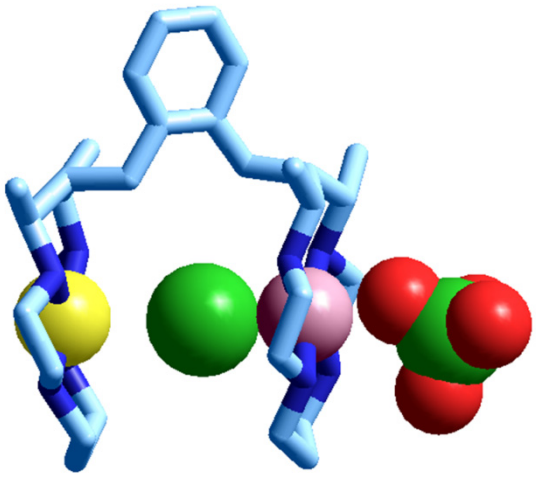

Figure 13. The crystal and molecular structure of the complex salt $[Ni^{II}_2(\mathbf{5})(\mu\text{-}Cl)(ClO_4)](ClO_4)_2{\cdot}H_2O$. Hydrogen atoms of the ligand, the two uncoordinated ClO_4^- ions and the solvational water molecule have been omitted for clarity.

Moreover, persistence of the absorption band of the yellow chromophore even in the presence of chloride excess suggests that in each step of anion complexation a mixture of high- and low-spin forms exists. On these bases, coordinative and geometrical aspects of the three stepwise equilibria are pictorially illustrated in Figure 14.

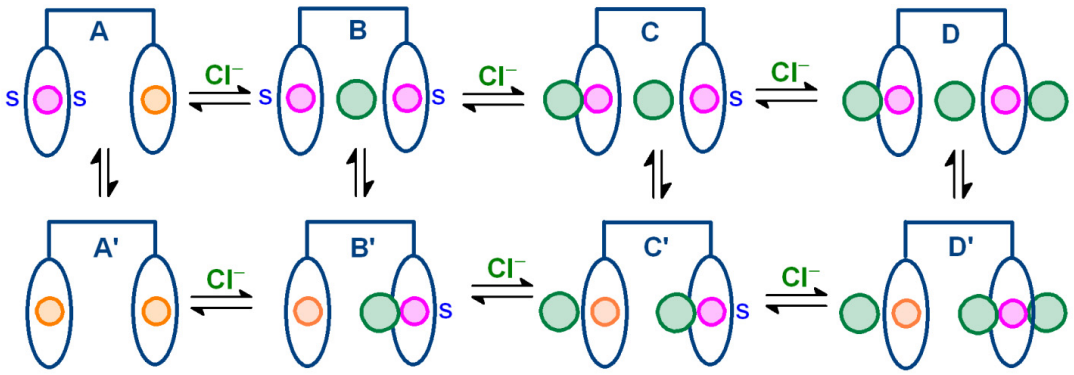

Figure 14. Hypothesized structural changes in the $[Ni_2^{II}(\mathbf{4})]^{4+}$ complex during titration with Cl^-.

In particular, the μ-Cl complex should exist as an equilibrium mixture of a fully paramagnetic species (B) and a mixed-valence form (B'). In the following steps, the concentration of the paramagnetic forms increase, to reach a steady value. Whether in the fully paramagnetic species B, C and D the intermetallic chloride ion lies at the same distance from the two metal center or is closer to one of them is only matter of speculation, in the absence of specific structural data.

It has to be notice that K_1 for the dinuclear complex $[Ni_2^{II}(\mathbf{4})]^{4+}$ is 32-fold higher than that observed for the mononuclear complex $[Ni^{II}(\mathbf{5})]^{2+}$ ($\Delta\log K_1 = 1.5$), pointing out to the existence of a *bimacrocyclic effect*. The corresponding energy advantage (8.6 kJ mol^{-1}) roughly reflects the

additional contribution of the interaction of Cl^- included in the inter-ring cavity with the facing low-spin Ni^{II} ion.

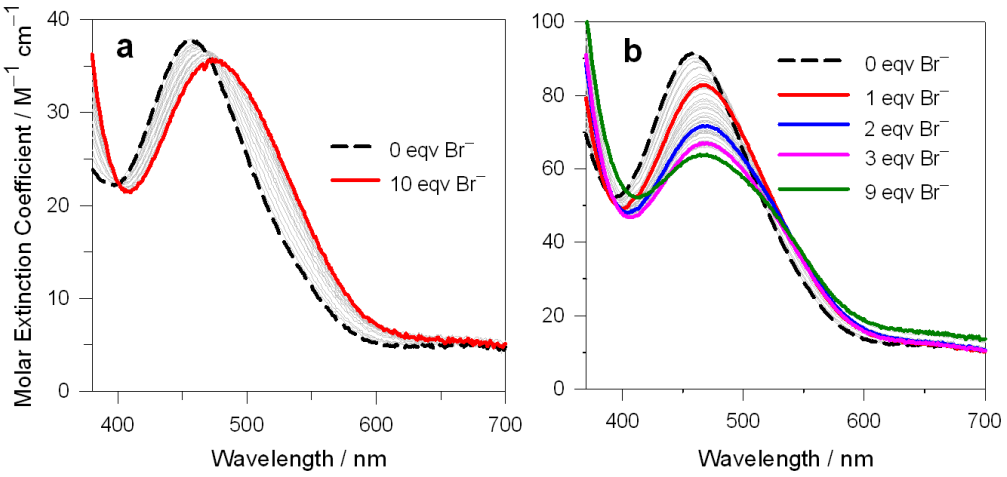

Figure 15. Spectra taken over the course of the titration with $[Bu_4N]Br$ of a DMSO solution (a) of $[Ni^{II}(\mathbf{5})](ClO_4)_2$, and (b) of $[Ni^{II}_2(\mathbf{4})](ClO_4)_4$, at 25 °C.

The mode of interaction of bromide with mono- and di-nuclear receptors is peculiar, as shown by the spectra shown in Figure 15. The monometallic complex $[Ni^{II}(\mathbf{5})]^{2+}$ interacts with Br^- in the same way as with iodide: (i) red-shift of the band of the yellow chromophore (see Figure 15a), which maintains its intensity; (ii) formation of a single receptor-anion complex, of 1:1 stoichiometry, whose association constant is reported in Table 1. The five-coordinate, probably square-pyramidal, complex, exists as an equilibrium mixture of the high- and low-spin form. On the other hand, the behavior of the dimetallic complex $[Ni_2^{II}(\mathbf{4})]^{4+}$ is similar to that observed with chloride: (i) the absorption band centered at 455 nm undergoes red-shift and a pronounced decrease in intensity of (see Figure 15b); (ii) best fitting of titration data was obtained by assuming the stepwise formation of three complexes: $[Ni_2L{\cap}LX]^{3+}$, $[Ni_2L{\cap}LX_2]^{2+}$ and $[Ni_2L{\cap}LX_3]^{+}$. Corresponding equilibrium constants are reported in Table 1.

Table 1. Log *K* values associated to the stepwise association equilibria of complexes $[Ni^{II}(\mathbf{5})]^{2+}$ and $[Ni_2^{II}(\mathbf{4})]^{4+}$ with halides and pseudohalides, in DMSO at 25° C. In parentheses the standard deviation on the last figure.

L = **5**	Cl^-	Br^-	I^-	NCO^-	NCS^-	N_3^-
$[NiL]^{2+} + X^- \leftrightarrows [NiLX]^+$	2.7(1)	2.34(2)	1.87(2)	4.51(1)	3.5(1)	2.54(6)
$[NiLX]^+ + X^- \leftrightarrows [NiLX_2]$	2.2(4)			4.2(3)	1.1(3)	2.6(1)
L∩L = **4**	Cl−	Br−	I−	NCO−	NCS−	N3−
[Ni2L∩L]4+ + X− ⇆ [Ni2L∩LX]3+	4.20(7)	3.05(4)	2.22(1)	4.51(2)	3.9(1)	2.7(1)
[Ni2L∩LX]3+ + X− ⇆ [Ni2L∩LX2]2+	2.5(1)	2.70(6)		4.07(5)	3.2(2)	2.1(3)
[Ni2L∩LX2]2+ + X− ⇆ [Ni2L∩LX3]+	1.5(2)	2.56(9)		3.31(8)	2.1(3)	1.2(3)

It is therefore suggested that the stepwise interaction of $[Ni_2^{II}(\mathbf{4})]^{4+}$ with bromide proceeds according to the scheme illustrated in Figure 13. A moderate bimacrocyclic effect exists ($\Delta\log K_1$ = 0.7), to which an energy contribution of 4 kJ mol^{-1} corresponds.

Pseudohalides display a different behavior from halides when interacting with both mononuclear $[Ni^{II}(\mathbf{5})]^{2+}$ and dinuclear $[Ni_2^{II}(\mathbf{4})]^{4+}$ complexes. Figure 16a shows the spectra taken over the course of the titration of a DMSO solution of $[Ni^{II}(\mathbf{5})](ClO_4)_2$ with $[Bu_4N]NCO$.

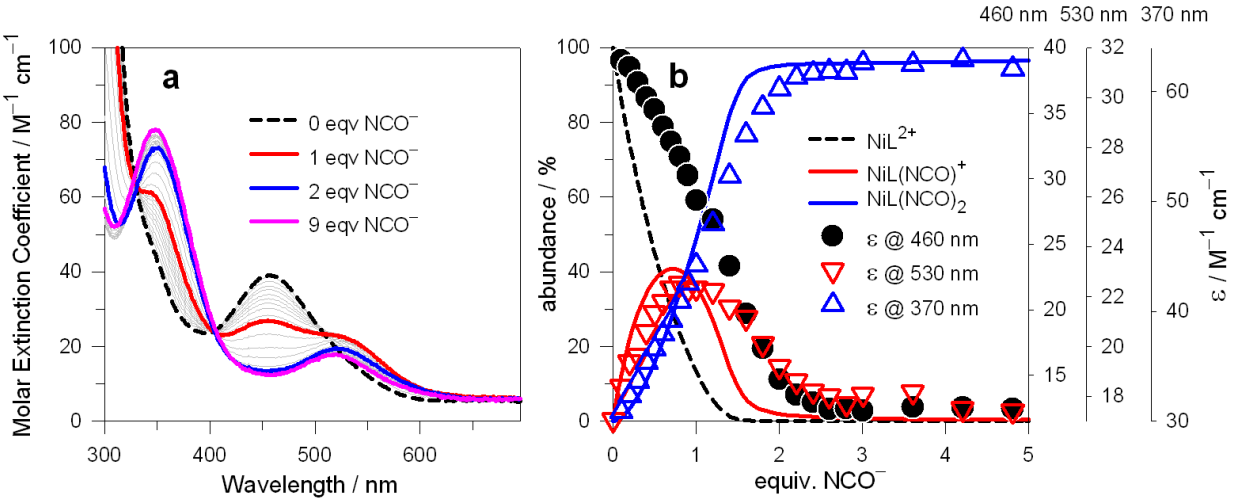

Figure 16. (a) Spectra taken over the course of the titration of a DMSO solution 5 × 10^{-3} M in $[Ni^{II}(\mathbf{5})](ClO_4)_2$ with $[Bu_4N]NCO$, at 25 °C; (b) symbols: Molar Extinction Coefficients (ε) taken at selected wavelengths; lines: concentration profiles of the complex species at the equilibrium over the course of the titration.

On cyanate addition, the band at 455 nm, low-spin complex, decreases, while new bands, pertinent to the high-spin form, develop at 370 nm and 530 nm, a behavior observed also on titration with chloride. However, on addition of 2 and more equiv. of NCO$^-$, the absorption of the yellow chromophore completely disappears. On these bases, $[Ni^{II}(\mathbf{5})]^{2+}$/NCO$^-$ interaction can be described by the scheme in Figure 17.

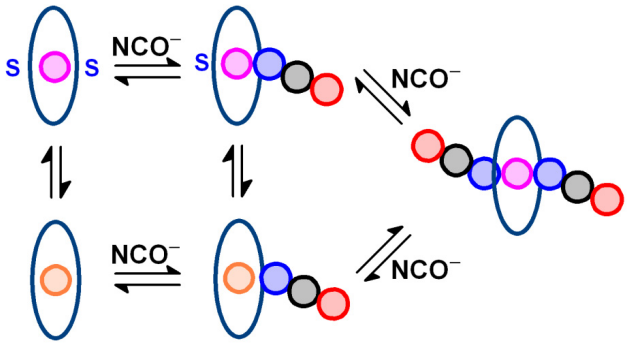

Figure 17. Hypothesized structural changes in the $[Ni^{II}(\mathbf{5})]^{2+}$ complex on titration with NCO$^-$.

In particular, on addition of the first equivalent of cyanate both a high-spin octahedral species and a low-spin five- or six-coordinate species forms, with the spin equilibrium displaced to the high-spin

complex. On addition of the second NCO^- equiv. the high-spin octahedral $[Ni^{II}(\mathbf{5})(NCO)_2]$ forms, which is present at 100%.

Figure 18a reports the spectra obtained on titration with NCO^- of a solution of the dinuclear complex $[Ni^{II}_2(\mathbf{4})](ClO_4)_4$.

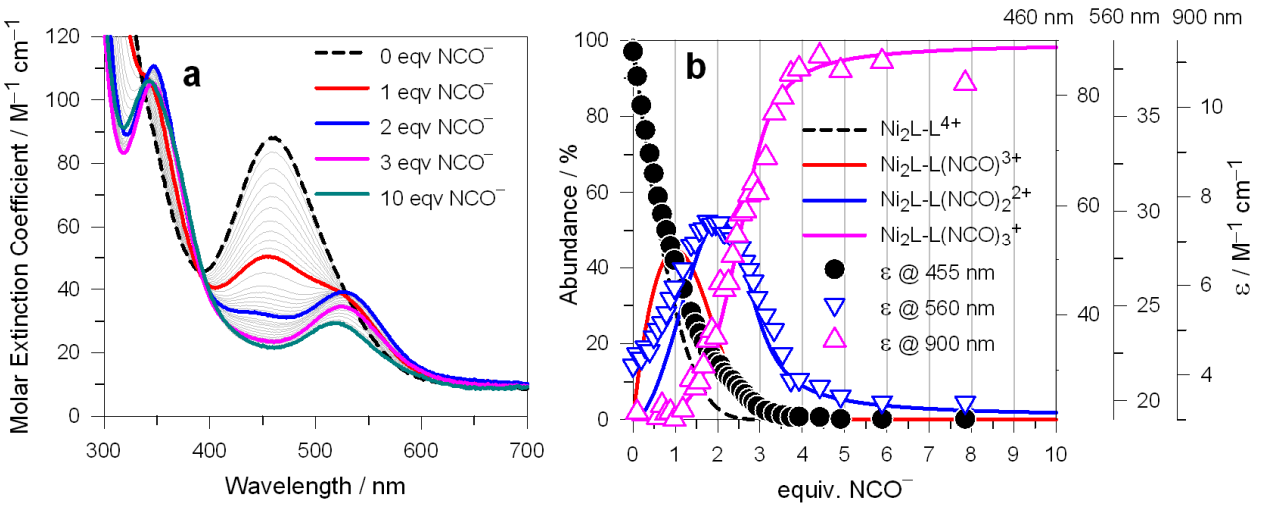

Figure 18. (a) Spectra taken over the course of the titration of a DMSO solution 5×10^{-3} M in $[Ni^{II}_2(\mathbf{4})](ClO_4)_4$ with $[Bu_4N]NCO$, at 25 °C; (b) symbols: Molar Extinction Coefficients (ε) taken at selected wavelengths; lines: concentration profiles of the complex species at the equilibrium over the course of the titration.

The spectral pattern is similar to that observed for the mononuclear complex, with a drastic decrease of the band of the yellow chromophore and the definite development of bands of the blue-violet chromophore at 350 and 530 nm. In particular, on addition of 2 equiv. of NCO^- and more the band at 455 nm (filled circles in Figure 18b) disappears and only high-spin species are present in solution. Best fitting of titration data was obtained on assuming the presence at the equilibrium of three species: $[Ni^{II}_2(L\cap L)Cl]^{3+}$, $[Ni^{II}_2(L\cap L)Cl_2]^{2+}$ and $[Ni^{II}_2(L\cap L)Cl_3]^{+}$. Corresponding $\log K$ values are reported in Table 1.

Also in this case, absorption spectra alone do not give definite information on the coordination site of the first anion, whether inner or outer with respect to the dinuclear complex. On the other hand, the only crystal structure available for complexes of **4**, $[Ni^{II}_2(\mathbf{4})(\mu\text{-}NCO)(NCO)_2]^+$ (this work) refers to 1:3 receptor/anion complex (see Figures 5 and 6). The absence of a bimacrocyclic effect ($\log K_1$ values are the same for both mono- and di-nuclear complexes would suggest external coordination of the first cyanate ion. More convincing information will be provided by voltammetric studies, described in the next Section.

Titrations with thiocyanate and azide of both $[Ni^{II}(\mathbf{5})](ClO_4)_2$ and $[Ni^{II}_2(\mathbf{4})](ClO_4)_4$ showed the same spectral features observed with cyanate (see pertinent spectra in Supplementary Information: Figures S3-S4). Corresponding log *K* values are reported in Table 1.

The Ni^{II}/Ni^{III} redox change in the absence and in the presence of coordinating and poorly reducing anions: electrochemical anion sensing. Encircling by cyclam of transition metal favors the attainment of unusually high oxidation states (Ni^{III},[19,20] Cu^{III},[21,22] Ag^{II},[23,24] Ag^{III},[25] and also Hg^{III},[26] as a red transient). Such a feature results from the capability of the 14-membered tetra-aza macrocycle to exert strong in-plane interactions, which raise the energy of the metal centered, essential antibonding orbital, from which the electron is removed on oxidation. In particular, the Ni^{II}-to-Ni^{III} oxidation process can be carried out both chemically and electrochemically, in an acidic aqueous solution and in media resistant to oxidation (MeCN, DMSO). The $[Ni^{III}(cyclam)]^{3+}$ complex which forms typically shows an elongated octahedral coordination geometry, with two solvent molecules or two anions occupying the axial positions of the distorted octahedron. The formation of an authentic Ni^{III} complex (d^7, low-spin) has been characterised in solution by ESR investigations.[27] The crystal structure of the complex salt $[Ni^{III}(cyclam)(MeCN)_2](CF_3SO_3)_3$ has been reported.[28]

Figure 20 shows the differential pulse voltammetry (DPV) profile obtained at a platinum microsphere working electrode for a DMSO solution 10^{-3} M in $[Ni^{II}(\mathbf{5})](ClO_4)_2$ and 0.1 M in $[Bu_4N]PF_6$ (black line).

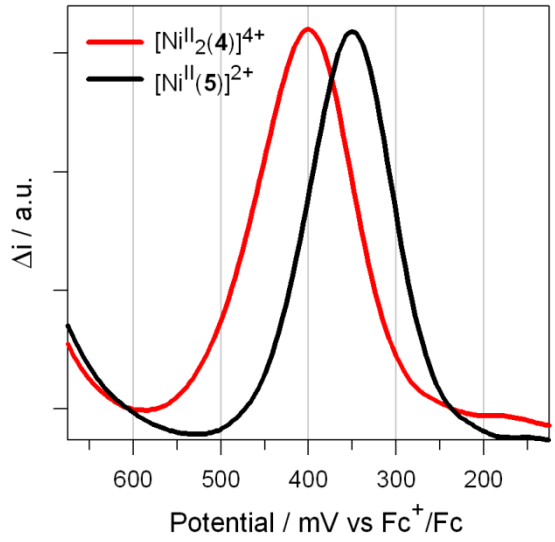

Figure 20. DPV profiles obtained at a platinum microsphere working electrode for a DMSO solution 0.1 M in $[Bu_4N]PF_6$ (pulse amplitude 20 mV). Black line: solution 10^{-3} M in $[Ni^{II}(\mathbf{5})](ClO_4)_2$; red line: solution 10^{-3} M in $[Ni^{II}_2(\mathbf{4})](ClO_4)_4$. Potential scan from less positive to more positive potentials (←). The intensities of the two profiles have been arbitrarily adjusted.

The oxidation peak ($E_{1/2}$ = 400 mV vs the internal Fc^+/Fc reference couple) shows a width at half maximum (δ) of 104 mV. The value expected for a fully electrochemically reversible one-electron redox change at 25 °C is 91 mV.[29] On the other hand, the red line in Figure 20 refers to the

oxidation behavior of the dinuclear complex salt $[Ni^{II}_2(\mathbf{4})](ClO_4)_4$. The observed single peak must be considered the convolution of two distinct peaks corresponding to the two stepwise one-electron oxidation processes:

$$[Ni^{II}–Ni^{II}(L\cap L)]^{4+} \leftrightarrows [Ni^{II}–Ni^{III}(L\cap L)]^{5+} + e^- \qquad (9)$$

$$[Ni^{II}–Ni^{III}(L\cap L)]^{4+} \leftrightarrows [Ni^{III}–Ni^{III}(L\cap L)]^{5+} + e^- \qquad (10)$$

In the case of two non-interfering and independent one-electron processes a single peak with $\delta = 91$ mV should be observed (for fully reversible electrochemical processes).[29] This corresponds to a $\Delta E_{1/2} = E_{1/2}(2) - E_{1/2}(1)$ difference of 36 mV (resulting from a purely statistical effect). Two peaks can be experimentally discerned in the DPV profile when $\Delta E_{1/2} \geq 80$ mV. In the present case, a δ value of 126 mV is observed, which, assuming full electrochemical reversibility, would give $\Delta E_{1/2} =$ 60 mV and, admitting a reversibility comparable to that of the mononuclear complex , $\Delta E_{1/2} \sim 50$ mV. Such a value should reflect a moderate electrostatic repulsion between the two positively charged metal centers. The existence of a minor repulsive effect is also demonstrated by the fact that the peak potential observed for the $[Ni^{II}(\mathbf{5})]^{2+}$ complex (350 mV vs Fc^+/Fc) is distinctly less positive than the peak potential for the $[Ni^{II}_2(\mathbf{4})]^{4+}$ complex (400 mV). In particular, the charge increase of each of the two Ni^{II} ions of the dinuclear complex is made slightly more difficult by the presence of a proximate positive charge.

Then, voltammetric studies have been carried out on DMSO solutions of $[Ni^{II}(\mathbf{5})](ClO_4)_2$ and of $[Ni^{II}_2(\mathbf{4})](ClO_4)_4$ (0.1 M in $[Bu_4N]PF_6$, 25 °C), in the presence of poorly reducing anions (Cl^-, NCO^-, N_3^-). Figure 21a shows the DPV profiles obtained over the course of the titration of a 10^{-3} M solution of the mononuclear complex salt $[Ni^{II}(\mathbf{5})](ClO_4)_2$ with $[Bu_4N]Cl$.

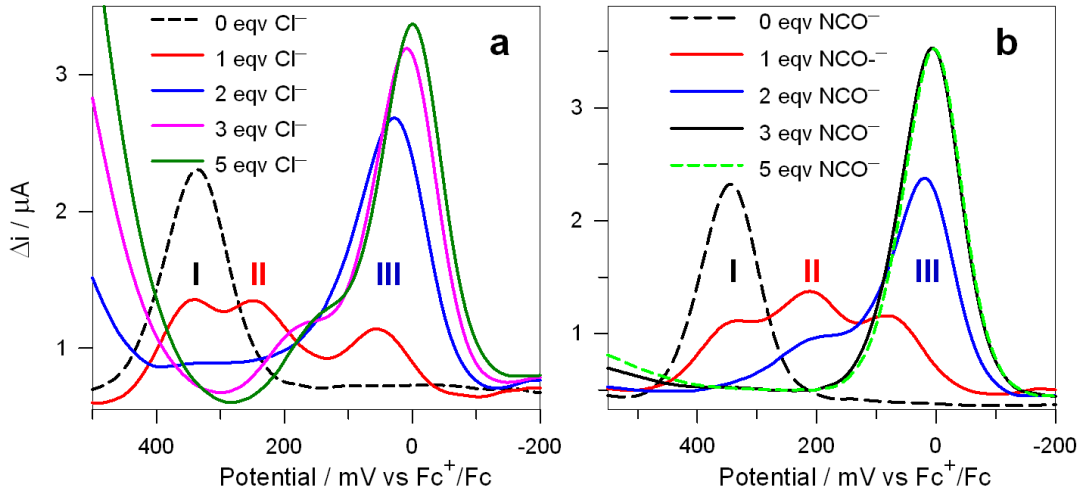

Figure 21. DPV profiles obtained at a platinum microsphere working electrode for a DMSO solution 10^{-3} M in $[Ni^{II}(\mathbf{5})](ClO_4)_2$ and 0.1 M in $[Bu_4N]PF_6$ (pulse amplitude 10 mV), to which up to 5 equiv. of $[Bu_4N]Cl$ (**a**) and $[Bu_4N]NCO$ (**b**) were added; potential scan from less positive to more positive potentials (←).

The development of the DPV profiles during titration can be interpreted on assuming the occurrence of the three stepwise half-reactions ($X^- = Cl^-$):

$$[Ni^{II}(L)]^{2+} \leftrightarrows [Ni^{III}(L)]^{3+} + e^- \qquad (11)$$

$$[Ni^{II}(L)X]^{+} \leftrightarrows [Ni^{III}(L)X]^{2+} + e^- \qquad (12)$$

$$[Ni^{II}(L)X_2] \leftrightarrows [Ni^{III}(L)X_2]^{+} + e^- \qquad (13)$$

It is observed that on addition of 1 equiv. of Cl^- (red line) a three-peak profile develops, due to the sequential occurrence of all three processes: (11) to which peak **I** corresponds, (12) (→ **II**), and (13) (→ **III**). On addition of further aliquots of chloride, peaks **I** and **II** progressively disappear, while peak **III** strengthens, according to a pattern roughly reproducing the change of concentration of the Ni^{II} complexes undergoing oxidation. The high intensity peak developing at more anodic potentials on addition of anion excess refers to the oxidation of unbound Cl^-.

Figure 21b displays the DPV profiles obtained on titration of $[Ni^{II}(\mathbf{5})](ClO_4)_2$ with $[Bu_4N]NCO$. The pattern is similar to that observed with chloride and, in the present case too, the three oxidation peaks have to be associated to eq. (11-13). Totally similar behavior was observed on titration a solution of $[Ni^{II}(\mathbf{5})](ClO_4)_2$ with $[Bu_4N]N_3$.

Figure 22a shows the DPV profiles obtained over the course of the titration of a 10^{-3} M solution of the dinuclear complex salt $[Ni^{II}_2(\mathbf{4})](ClO_4)_4$ with $[Bu_4N]Cl$.

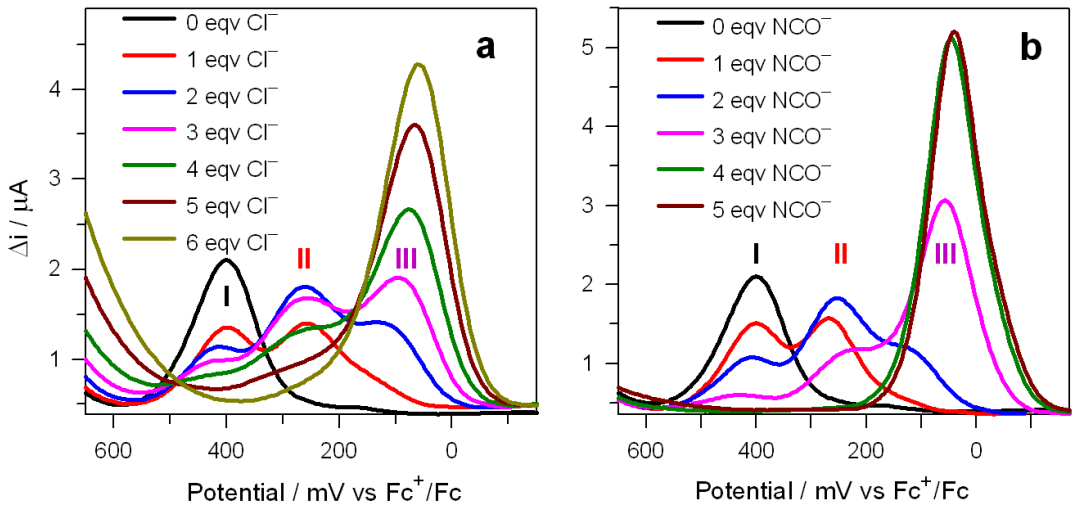

Figure 22. DPV profiles obtained at a platinum microsphere working electrode for a DMSO solution 10^{-3} M in $[Ni^{II}_2(\mathbf{4})](ClO_4)_4$ and 0.1 M in $[Bu_4N]BF_4$ (pulse amplitude 10 mV), to which up to 5 equiv. of $[Bu_4N]Cl$ (**a**) and $[Bu_4N]NCO$ (**b**) were added; potential scan from less positive to more positive potentials.

The DPV pattern consists of three peaks, a circumstance which seems inconsistent with the occurrence of the expected four half-reactions reported below ($X^- = Cl^-$):

$$[Ni^{II}_2(L\cap L)]^{4+} \leftrightarrows [Ni^{III}_2(L\cap L)]^{6+} + 2e^- \qquad (14)$$

$$[Ni^{II}_2(L\cap L)X]^{3+} \leftrightarrows [Ni^{III}_2(L\cap L)X]^{5+} + 2e^- \quad (15)$$

$$[Ni^{II}_2(L\cap L)(X)_2]^{2+} \leftrightarrows [Ni^{III}_2(L\cap L)(X)_2]^{4+} + 2e^- \quad (16)$$

$$[Ni^{II}_2(L\cap L)(X)_3]^{+} \leftrightarrows [Ni^{III}_2(L\cap L)(X)_3]^{3+} + 2e^- \quad (17)$$

The apparent paradox can be cleared on assuming that: (i) peak **I** corresponds to eq. (14), in which the two Ni^{II} centers (belonging to the forms **A** and **A'**, see Figure 13) are oxidized at nearly the same potential; (ii) peak **II** corresponds to eq. (15), in which it is the $[Ni^{II}_2(L\cap L)\mu\text{-}Cl]^{3+}$ complex (**B** and **B'** in Figure 13) that undergoes two-electron oxidation; (iii) peak **III** is the convolution of the two peaks corresponding to the half-reactions (16) and (17): the two equilibria refer to the concurring oxidation of complexes with a rather similar coordinative array (**C** and **C'**, then **D** and **D'** in Figure 13) and should be characterized by not too different $E_{1/2}$ values.

Figure 22b shows the family of DPV profiles obtained on voltammetric titration of the dinuclear complex with cyanate ion, which show a three-peak behavior as observed for titration with chloride. However, the pattern for NCO^- is not exactly the same as for Cl^-. In particular, for Cl^- peak **III** develops significantly since the addition of the 2nd equiv. of anion (blue line in Figure 22a). On the other hand, in the case of cyanate, peak **III** grows significantly only on addition of the 4th equiv. of anion and fully develops with the 5th equiv. (brown line in Figure 22b). Such a different behavior can be interpreted on assuming that: (i) first, the oxidation of the complexes $[Ni^{II}_2(L\cap L)NCO]^{3+}$ (**B** in Figure 23) and $[Ni^{II}_2(L\cap L)(NCO)_2]^{2+}$ (**C** in Figure 23), in which cyanate ions are externally coordinated to the two Ni^{II} centers, takes place; therefore, peak **II** should be considered the convolution of two peaks with close $E_{1/2}$; (ii) then, it is the turn of the $[Ni^{II}_2(L\cap L)(\mu\text{-}NCO)(NCO)_2]^{+}$ complex (**D** in Figure 23), in which the 3rd NCO^- ion went to occupy the intermetallic cavity, a process producing peak **III**. Thus, voltammetric titration enables us to propose a sound mechanistic sequence for the stepwise uptake of three cyanate ions by the dinuclear receptor $[Ni^{II}_2(\mathbf{4})]^{4+}$ in DMSO, which is pictorially illustrated in Figure 23.

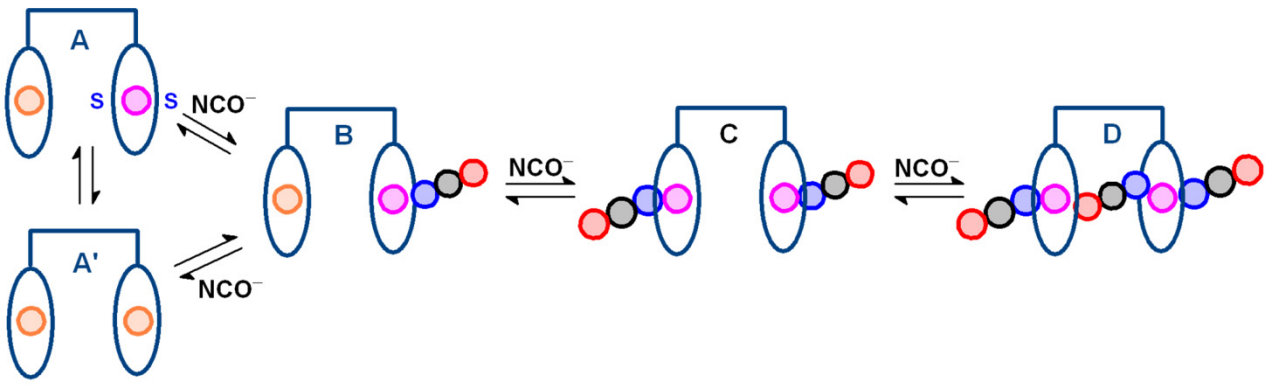

Figure 23. Hypothesized structural changes in the $[Ni_2^{II}(\mathbf{4})]^{4+}$ complex during titration with NCO^-.

Failure of the first cyanate ion to occupy the intermetallic cavity according should be ascribed to two main factors: (i) the intrinsic difficulty of the triatomic anion to accomodate itself in the inner room and to fulfill the geometrical requirements associated to hybridization of terminal donor atoms; (ii) the less pronounced coordinating tendency of the terminal oxygen atom of NCO^- with respect to terminal nitrogen atom. Such a feature is confirmed by the large Ni^{II}–O distance (2.30 Å) compared to Ni^{II}–N (2.15 Å). As a consequence, first and second NCO^- choose to bind Ni^{II} ions externally, thus profiting by coordination of nitrogen atoms according to a geometrical arrangement free of steric constraints.

The model illustrated in Figure 23 can be proposed also for the interaction of $[Ni^{II}_2(\mathbf{4})]^{4+}$ with N_3^-, for which a pattern of voltammetric profiles similar to that of NCO^- was observed (see Figure S8 in Supplementary Information). Moreover, the scheme in Figure 23 should be valid also for the interaction of $[Ni^{II}_2(\mathbf{4})]^{4+}$ with NCS^-, which was spectrophotometrically, but not voltammetrically investigated, due to the poor resistance of thiocyanate to oxidation at platinum electrode.

Further information on the oxidation mechanism can be obtained The separation of each couple of DPV peaks ΔE is expressed by the following equation:

——— ——— (18)

where $K_i(Ni^{II})$ is the equilibrium constant for the i^{th} step of complexation for the Ni^{II} complex: $[Ni^{II}LX_i]^{(2-1)+} + X^- \leftrightarrows [Ni^{II}LX_{1+i}]^{(1-i)+}$, and $K_i(Ni^{III})$ is the equilibrium constant for the i^{th} step of complexation for the Ni^{III} complex: $[Ni^{III}LX_i]^{(3-i)+} + X^- \leftrightarrows [Ni^{III}LX_{1+i}]^{(2-i)+}$ (i = 1, 2). N is the number of electrons involved in the redox process. The ratio $K_i(Ni^{III})/K_i(Ni^{II})$ is called Enhancement Factor (EF) and defines the effect of complexation (e.g. by Cl^-) on the stabilization of the Ni^{III} state.[30] The larger the peak separation, the higher the stability of the complex of the oxidised receptor with respect to the reduced one. Values of ΔE for the complexation of the mono- and di-nuclear complexes by Cl^- and NCO^- can be visually evaluated in the diagram in Figure 24.

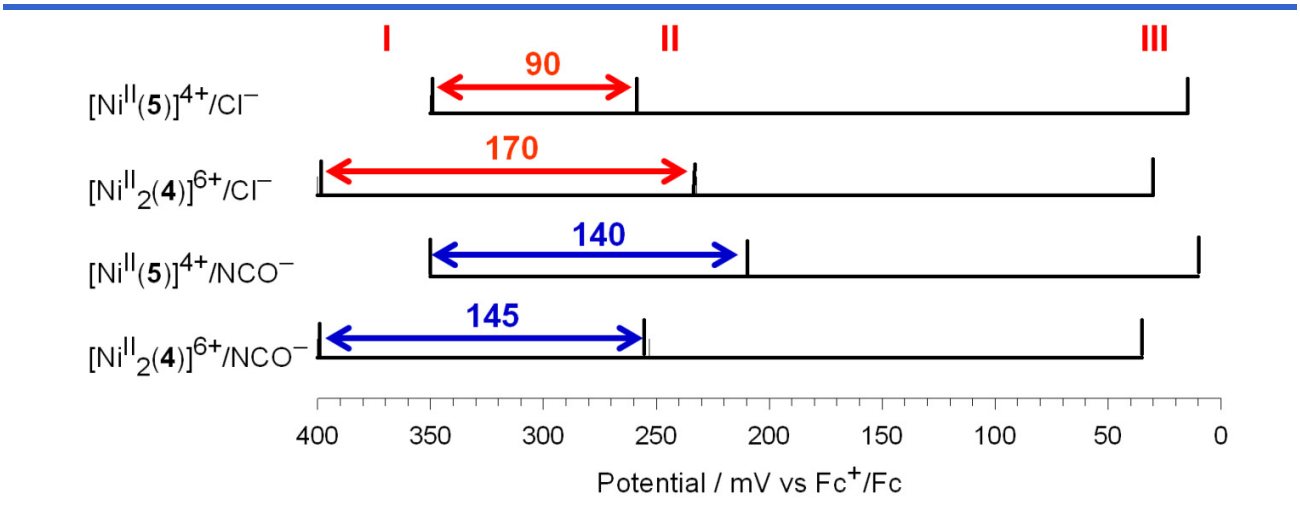

Figure 24. Linear representation of peak potentials determined over the course of the DPV titrations of $[Ni^{II}(\mathbf{5})]^{2+}$ and $[Ni_2^{II}(\mathbf{4})]^{4+}$ with Cl^- and NCO^-. The larger the peak separation, the higher the stability of the complex of the oxidised receptor (Ni^{III}) with respect to the reduced one (Ni^{II}).

As far ΔE(I-II) differences are concerned, the following features are observed:

1. for NCO^-, ΔE(I-II) values are nearly the same for both the the mononuclear and dinuclear complexes, as well as EF values (232 and 282). This is consistent with the fact that in the two complexes the first NCO^- interacts with only one metal center, thus exerting the same stabilization effect on the trivalent state, of mere ligand field origin (the tripositive metal ion experiences a Ligand Field Stabilization Energy higher than the dipositive one).
2. for Cl^-, ΔE(I-II) for the dinuclear complex is remarkably larger than for the mononuclear complex (170 and 90 mV, respectively, to which EF values of 750 and 33 correspond)). The huge stabilization results from the additional contribution due to the shielding of the intermetallic electrostatic repulsion by the first chloride ion occupying the inner room of the dinuclear receptor.

Strange case of NO_3^-, which binds only Ni^{III} in a bicyclam arrangement. Titration of DMSO solutions of $[Ni^{II}(\mathbf{5})]^{2+}$ and of $[Ni^{II}_2(\mathbf{4})]^{4+}$ with $[Bu_4N]NO_3$ did of not cause any modification of the absorption spectra, indicating no interaction of the anion with the divalent metal. Moreover, the DPV profile of the $[Ni^{II}(\mathbf{5})]^{2+}$ complex was not altered following the addition of nitrate, which demonstrated that also the trivalent mononuclear complex does not shows any affinity towards NO_3^-. On the other hand, when $[Bu_4N]NO_3$ was added to a DMSO solution of $[Ni^{II}_2(\mathbf{4})]^{4+}$, the DPV peak at 400 mV, progressively moved towards less positive potentials (see Figure 25a).

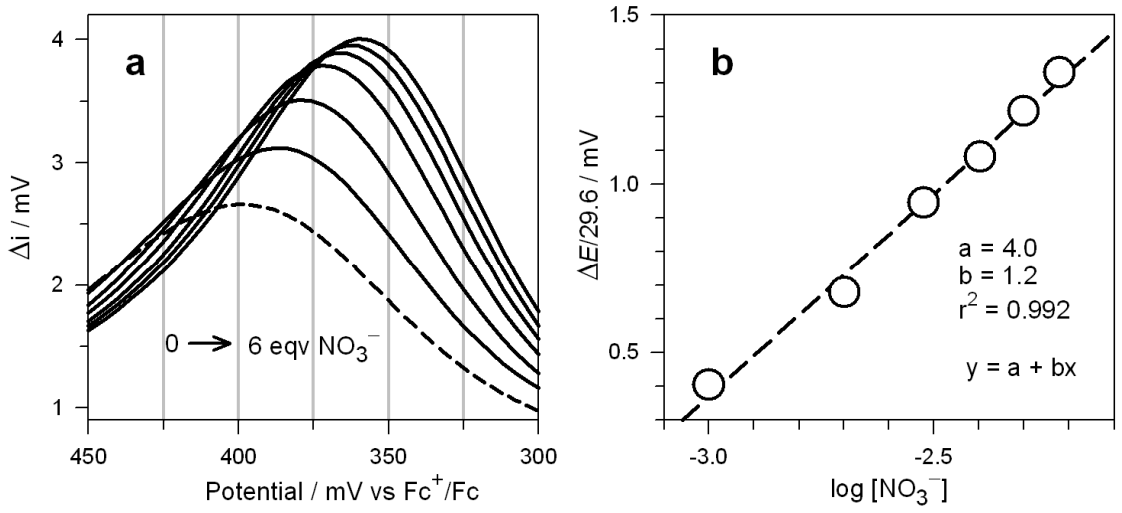

Figure 25. (a) DPV profiles obtained at a platinum microsphere working electrode for a DMSO solution 10^{-3} M in $[Ni^{II}_2(\mathbf{4})](CF_3SO_3)_4$ and 0.1 M in $[Bu_4N]PF_6$ (pulse amplitude 20 mV), to which 1, 2, 3, 4, 5, 6 equiv. of $[Bu_4N]NO_3$ were added; (b) plot of $\Delta E/29.6$ vs $\log[NO_3^-]$ disclosing a linear correlation which roughly

corresponds to the equation: $\Delta E/29.6 = K(\mathrm{III}) + \log[NO_3^-]$. $K(\mathrm{III})$ is the association constant of the 1:1 complex $[Ni^{III}_2(\mathbf{4})(NO_3)]^{5+}$.

Such a behavior is expected for a redox system M^+/M in which only the oxidized form M^+ interacts with X^-, according to the equilibrium $M^+ + X^- \leftrightarrows [MX]$, whose constant is K^+. In particular, the difference of the peak potential in the absence (ΔE) and in the presence of X^- is related to the molar concentration $[X^-]$ according to the equation:[31,32]

$$\Delta E = \frac{59.16}{n} K^+ + 59.16 \log[X^-] \qquad (19)$$

Considering that we are in the presence of a two-electron process ($n = 2$), equation (18) must be rearranged to

$$\frac{\Delta E}{29.6} = K^+ + \log[X^-] \qquad (20)$$

Indeed, plotting of ΔE(mV)/29.6 vs $\log[X^-]$ gives a straight line (Figure 25b), whose slope reasonably approaches unity and whose intercept (4) is K^+ (i.e. the constant of the equilibrium: $[Ni^{III}_2(\mathbf{4})]^{6+} + NO_3^- \leftrightarrows [Ni^{III}_2(\mathbf{4})(NO_3)]^{5+}$).

The fact that the $[Ni^{II}(\mathbf{5})]^{2+}/[Ni^{III}(\mathbf{5})]^{3+}$couple does not sense NO_3^- and the $[Ni^{II}_2(\mathbf{4})]^{4+}/[Ni^{III}_2(\mathbf{4})]^{6+}$ does indicate that the poorly coordinating nitrate ion is not able to bind any Ni^{III}-cyclam subunit externally. It is therefore suggested that NO_3^- goes into the inner cavity of $[Ni^{III}_2(\mathbf{4})]^{6+}$ to profit from the interaction with the two metallocyclam subunits, a further evidence of the *bimacrocyclic effect*.

■ CONCLUSION

In the absence of serious steric constraints, receptors containing unsaturated metal centers uptake anions according to an affinity sequence which reflects the spectrochemical series, i.e. the ligand field effect exerted by each anion. This is surely the case of the mononuclear $[Ni^{II}(\mathbf{5})]^{2+}$ complex, for which K_1 decreases along the series: $NCO^- > Cl^- > N_3^- > Br^- > NCS^- > I^-$. The same trend is observed for the dinuclear $[Ni_2^{II}(\mathbf{4})]^{4+}$, but the ligand field effect varies with the nature of the anion.

In Figure 26 we have plotted $\log K_1$ for the dinuclear complex vs. $\log K_1$ value for the mononuclear complex.

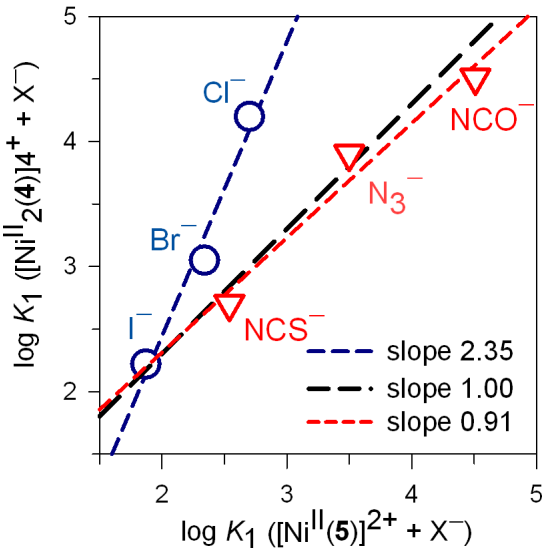

Figure 26. Plot of log K_1 for $[Ni_2^{II}(\mathbf{4})]^{4+}$ vs. log K_1 value for the $[Ni^{II}(\mathbf{5})]^{2+}$. Black dashed line refers to an ideal behavior in which ligand field effects are the same for both mononuclear and dinuclear complexes, in the absence of steric constraints: log $K_1([Ni_2^{II}(\mathbf{4})]^{4+})$ = 2.3 + log $K_1([Ni^{II}(\mathbf{5})]^{2+})$

If the anion affinity were the same for both receptors, values should lie on the same straight-line with slope = 1.00. We observe that pseudohalides lie on a straight-line whose slope (0.91) is very close to unity, whereas halides lie on a straight-line of much greater slope (2.35). Such a behavior seems to agree with the structural hypotheses put forward for the interaction of the receptor with the first anion: (i) pseudohalides profit from coordination to the same extent whether they bind the metal center of the mononuclear complex or the dinuclear complex (which takes place externally); (ii) halides profit from coordination to a greater extent when binding the dinuclear receptor because they are included in the intermetallic cavity and interact with two metal centers.

Most of metal-based receptors contain copper(II) in view of several convenient features of the metal ion: (i) geometrical versatility, (ii) leading position in the Irving-Williams series,[33] (iii) relatively high molar extinction coefficient (ε) of its complexes (e.g. with polyamines, ε > 100 M^{-1} cm^{-1}). The Ni^{II} ion does not show similar favorable characteristics and, in particular, forms weakly colored polyamine complexes (ε < 10). The metallocyclam subunit of $[Ni_2^{II}(\mathbf{4})]^{4+}$ is different due to the coexistence in solution a the light-blue form (ε < 10 for bands in the visible region) and of a bright yellow form (ε 50−100 M^{-1} cm^{-1}, at ~ 500 nm). In particular, the blue-to-yellow interconversion is highly sensitive to axial binding by exotic ligands and allows a convenient monitoring of anion binding. Moreover, when encircled by cyclam-like ligands, Ni^{II} displays a rich redox activity (e.g. easy oxidation to Ni^{III}), which is strongly affected by anion coordination, thus providing a second channel for analyte detection. Studies on the design of dinickel(II) complexes with bicyclam ligands with increased steric constraints are underway in our Laboratory.

■ EXPERIMENTAL SECTION

General Procedures and Materials. All reagents and solvents were supplied by Aldrich and used as received. UV−Vis spectra were recorded on a Varian CARY 50 spectrophotometer with

quartz cuvette of 1 cm path length. UV-Vis titrations were carried out at 25 °C on 5×10^{-3} M solutions of $[Ni^{II}_2(\mathbf{4})](ClO_4)_4$ and $[Ni^{II}(\mathbf{5})](ClO_4)_2$ in DMSO, by adding aliquots of freshly prepared standard solutions (in DMSO) of $[Bu_4N]X$ (X = Cl, Br , I , NCO , NCS and N_3). Titration data were processed with the Hyperquad software to determine the equilibrium constants.[17] HySS programm was used to obtain the distribution diagrams of the species.[34]

Differential-pulse voltammetry (DPV) measurements were performed in a conventional three-electrode cell, using a PAR 273 potentiostat/galvanostat controlled by a PC and driven by dedicated software. A platinum microsphere and a platinum foil were used as working and counter electrodes, respectively, while an Ag/AgCl wire, dipped in a solution of $AgNO_3$ in DMSO, was the reference electrode. $[Bu_4N]PF_6$ (0.1 M) was used as a supporting electrolyte. Potential values were then referred to the potential of the Fc^+/Fc couple, whose $E_{1/2}$ value was measured at the end of each DPV titration, after the addition of ferrocene to the DMSO solution. The potential scan rate in the DPV experiments was 20 mV s^{-1}. DPV titrations were carried out by adding aliquots of freshly prepared standard solutions (in DMSO) of $[Bu_4N]X$ (X = Cl, Br , I , NCO , NCS and N_3 to DMSO solutions 10^{-3} M of $[Ni^{II}_2(\mathbf{4})](ClO_4)_4$ and $[Ni^{II}(\mathbf{5})](ClO_4)_2$, at 25 °C.

Mass spectra were acquired on a Thermo-Finnigan ion trap LCQ Advantage Max instrument, equipped with an ESI source. Elemental analyses were carried out using a Costech ECS 4010 instrument at the Department of Chemistry, Materials, and Chemical Engineering "G. Natta", Politecnico di Milano, Milan, Italy.

[(5,7-Dimethyl-6-benzyl-1,4,8,11-tetraazacyclotetradecane)-nickel(II)] Perchlorate, $[Ni^{II}(\mathbf{5})](ClO_4)_2$. The complex salt was prepared according to a previously described procedure.[35] Anal. Calcd for $C_{19}H_{34}Cl_2N_4NiO_8$ (PM = 576.09): C, 39.6; H, 5.9; N, 9.7. Found: C, 39.4; H, 6.0; N, 9.6.MS (CH_3OH, ESI): m/z 188.2 (100%; $[Ni^{II}(\mathbf{5})]^{2+}$), 475.4 (20% $[Ni^{II}(\mathbf{5}) + ClO_4^-]^+$). UV−vis [Acetone, λ_{max} nm (ε, M^{-1} cm^{-1})]: 468 (62).

α,α'-Bis[(5,7-dimethyl-1,4,8,11-tetraazacyclotetradecan-6-yl)-nickel(II)]-o-xylene Perchlorate, $[Ni^{II}_2(4)](ClO_4)_4$. The complex salt was prepared according to a previously described procedure,[10] and dried under vacuum at 50 °C. Anal. Calcd for $C_{32}H_{62}Cl_4N_8Ni_2O_{16}$ (PM = 1074.08): C, 35.8; H, 5.8; N, 10.4. Found: C, 35.6; H, 5.7; N, 10.1. MS (CH_3OH, ESI): m/z 336.4 (40%, $[Ni^{II}_2(\mathbf{4}) -2H^+]^{2+}$), 386.3 (100%, $[Ni^{II}_2(\mathbf{4}) -H^+ +ClO_4^-]^{2+}$. UV−vis [acetone] λ_{max} nm (ε, M^{-1} cm^{-1})]: 468 (124)

Safety note! *Perchlorate salts of metal complexes are potentially explosive and should be handled with care. In particular, they should never be heated as solids.*

X-ray crystallographic studies. Diffraction data for $[Ni^{II}_2(\mathbf{4})(\mu\text{-}NCO)(NCO)_2]ClO_4 \cdot 2.5H_2O$ (violet, 0.41 × 0.12 × 0.10 mm^3) have been collected by means of a

Bruker-Axs CCD-based three circle diffractometer, working at ambient temperature with graphite-monochromatized Mo Kα X-radiation (λ = 0.71073 Å). Data reduction was performed with the *SAINT* software,[36] and intensities were corrected for Lorentz and polarization effects. Absorption effects were empirically evaluated by the *SADABS* software,[37] and absorption correction was applied to the data. Crystal structure was solved by direct methods (*SIR 97*)[38] and refined by full-matrix least-square procedures on F^2 using all reflections (*SHELXL 97*).[39] Anisotropic displacement parameters were refined for all non-hydrogen atoms. Hydrogens bonded to C atoms were placed at calculated positions with the appropriate AFIX instructions and refined using a riding model. Hydrogens bonded to secondary amines were located in the final ΔF maps and their positions were successively refined restraining the N-H distance to be 0.90 ± 0.01 Å. Positions for hydrogens belonging to water solvent molecules remained undetermined. Perchlorate counterion was disordered over two alternative positions having three O-atom positions in common. The remaining O and Cl atom positions were mutually exclusive and half populated. A partly present water solvent molecule occurred in the half populated O(3w) site when the Cl(1b) and O(7b) alternative atom positions were not populated.

Crystal data for $[Ni^{II}_2(\mathbf{4})(\mu\text{-NCO})(NCO)_2]ClO_4\cdot 2.5H_2O$: $C_{35}H_{67}ClN_{11}Ni_2O_{9.5}$, M = 946.87, monoclinic, $P\ 2_1/n$ (no. 14), a = 9.5464(5) Å, b = 25.5845(12) Å, c = 18.1421(9) Å, β = 90.9118(9)°, V = 4430.5(4) Å^3, Z = 4, 46001 measured reflections, 9656 unique reflections (R_{int} 0.038), 6975 strong data [$I_O>2\sigma(I_O)$], 0.0507 and 0.1314 $R1$ and $wR2$ for strong data, 0.0722 and 0.1483 $R1$ and $wR2$ for all data.

■ ASSOCIATED CONTENT

Supporting information

X-ray crystallographic files in CIF format and plots showing thermal ellipsoids for the studied molecular crystals. Further details on the spectrophotometric and voltammetric titrations in DMSO. This material is available free of charge via the Internet at http://pubs.acs.org.

■ AUTHOR INFORMATION

Corresponding Author:

* E-mail: luigi.fabbrizzi@unipv.it

■ ACKNOWLEDGEMENTS

The financial support of the Italian Ministry of University and Research (PRIN–InfoChem) is gratefully acknowledged.

■ REFERENCES

(1) Bowman-James, K.; Bianchi, A.; E. García-Espana, E. (Eds) *Anion Coordination Chemistry*, John Wiley & Sons, New York, 2012.

(2) Schmidtchen, F. P.; Berger M. *Chem. Rev.* **1997**, *97*, 1609−1646.

(3) Amendola, V.; Fabbrizzi, L. *Chem. Commun.* **2009**, 513–531.

(4) Fabbrizzi, L.; Poggi, A. *Chem. Soc. Rev.* **2013**, *42*, 1681−1699.

(5) Alibrandi, G.; Amendola, V.; Bergamaschi, G.; Fabbrizzi, L.; Licchelli, M. *Org. Biomol. Chem.* **2015**,*13*, 3510−3524.

(6) Fabbrizzi, L.; Leone, A.; Taglietti, A. *Angew. Chem. Int. Ed.* **2001**, *40*, 3066−3069.

(7) Murase, I.; Mikuriya, M.; Sonoda, H.; Fukuda, Y.; Kida, S. *J. Chem. Soc. Dalton Trans.* **1986**, 1953

(8) (a) (C-C linked bicyclams): Fabbrizzi, L.; Montagna, L.; Poggi, A.; Kaden, T. A.; Siegfried, L. C. *Inorg. Chem.* **1986**, *25*, 2671-2672; (N-N linked bicyclams): Ciampolini, M.; Fabbrizzi, L.; Perotti, A.; Poggi, A.; Seghi, B.; Fabrizio Zanobini, F. *Inorg. Chem.*, **1987**, *26*, 3527–3533.

(9) Kajiwara, T.; Yamaguchi, T.; Kido, H.; Kawabuta, S.; Kuroda, R.; Ito, T. *Inorg. Chem.* **1993**, *32*, 4990-4991; Kajiwara, T.; Yamaguchi, T.; Oshio, H.; Ito, T. *Bull. Chem. Soc. Jpn.***1994**, *67*, 2130−2135.

(10) Szacilowski, K. T.; Xie, P.; Malkhasian, A. Y. S.; Heeg, M. J.; Udugala-Ganehenege, M. Y.; Wenger, L. E.; Endicott, J. F. *Inorg. Chem.* **2005**, *44*, 6019−6033.

(11) Anichini, A.; Fabbrizzi, L.; Paoletti, P.; Clay, R. M. *Inorg. Chim. Acta*, **1977**, *24*, L21−L22.

(12) Sabatini, L.; Fabbrizzi, L. *Inorg. Chem.*, **1979**, *18*, 438−444.

(13) Bosnich, B.; Poon, C. K.; Tobe, M. L. *Inorg. Chem.* **1965**, *4*, 1102–1108.

(14) Liang, X.; Sadler, P. J. *Chem. Soc. Rev.* **2004**, *33*, 246–266.

(15) Adam, K. R.; Antolovich, M.; Brigden, L. G.; Leong, A. J.; Lindoy, L. F.; Baillie, P. J.; Uppal, D. K.; McPartlin, M.; Shah, B.; Proserpio, D.; Fabbrizzi, L.; Tasker, P. A. *J. Chem. Soc., Dalton Trans.* **1991**, 2493−2501.

(16) Valach, F.; Dunaj-Jurco, M. *Acta Crystallogr.* **1982**, *B38*, 2145−2148.

(17) 'Hyperquad 2013' package; Gans, P.; Sabatini, A.; Vacca, A. *Talanta* **1996**, *43*, 1739–1753; http://www.hyperquad.co.uk/HQ2013.htm ; accessed 2 December, 2015.

(18) Hinz, F. P.; Margerum, D. W. *Inorg. Chem.* **1974**, 13, 2941–2949.

(19) Olson, D. C., J. Vasilevskis, J. *Inorg. Chem.* **1968**, *8*, 1611–1621.

(20) Bencini, A.; Fabbrizzi, L.; Poggi, A. *Inorg. Chem.* **1981**, 20, 2544–2549.

(21) Olson, D. C., J. Vasilevskis, J. *Inorg. Chem.***1971**, *10*, 463–470.

(22) Bisi Castellani, C., Fabbrizzi, L., Licchelli, M., Perotti, A., Poggi, A. *J. Chem. Soc., Chem. Comm.* **1984**, 806−808.

(23) Kestner, M. O., Allred, A, L. *J. Am. Chem. Soc.* **1972**, *94*, 7189–7189.

(24) Barefield, E. K., Mocella, M. T. *Inorg. Chem.* **1973**, *12*, 2829–2832.

(25) Pesavento, M., Profumo, A., Soldi, T., Fabbrizzi, L. *Inorg. Chem.* **1985**, *24*, 3873–3875.

(26) Deming, R. L.; Allred, A. L.; Dahl, A. R.; Herlinger, A. W.; Kestner, M. O. *J. Am. Chem. Soc.* **1976**, *98*, 4132–4137

(27) LoVecchio, F. V.; Gore, E. S.; Busch, D. H. *J. Am. Chem. Soc.***1974**, *96*, 3109–3118.

(28) Nishigaki, J.; Matsumoto, T.; Tatsumi, K. *Inorg. Chem.* **2012**, *51*, 3690−3697.

(29) Richardson, D. E.; Taube, H. *Inorg. Chem.* **1981,** *20,* 1278−1285.

(30) Amendola, V.; Fabbrizzi, L.; Mosca, L. *Chem. Soc. Rev.* **2010**, *39*, 3889–3915.

(31) Miller, S. R.; Gustowski, D. A.; Chen, Z.-H.; Gokel, G. W.; Echegoyen, L.; Kaifer, A. E. *Anal. Chem.* **1988**, *60*, 2021–2024.

(32) Amendola, V.; Boiocchi, M.; Colasson, B.; Fabbrizzi, L.; Monzani, E.; Douton-Rodriguez, M.-J.; Spadini, C. *Inorg. Chem.* **2008**, *47*, 4808−4816.

(33) Irving, H. M. N. H.; Williams, R. J. P. *J. Chem. Soc.* **1953**, 3192–3210.

(34) 'HySS 2009' package; Alderighi, L.; Gans, P.; Ienco , A.; Peters, D.; Sabatini, A.; Vacca, A. *Coord. Chem. Rev.* 1999, *184*, 311−318; http://www.hyperquad.co.uk/hyss.htm, accessed 2 December, 2015.

(35) DeRosa, F.; Bu, X.; Pohaku, K.; Ford, P. *Inorg. Chem.* **2005**, *44*, 4166−4174.

(36) *SAINT Software Reference Manual*, Version 6; Bruker AXS Inc.: Madison, WI, 2003.

(37) Krause, L.; Herbst-Irmer, R.; Sheldrick, G.M.; Stalke, D. *J. Appl. Crystallogr*. **2015**, *48*, 3−10.

(38) Altomare, A.; Burla, M. C.; Camalli, M.; Cascarano, G. L.; Giacovazzo, C.; Guagliardi, A.; Moliterni, A. G. G.; Polidori, G.; Spagna, R. *J. Appl. Crystallogr*. **1999**, *32*, 115−119.

(39) Sheldrick, G. M. *Acta Crystallogr*. **2008**, *A64*, 112−122.